STEM CELLS AND DEVELOPMENT
Volume 23, Number 23, 2014

DOI: 10.1089/scd.2014.0058

Pax6 Is Essential for the Maintenance and Multi-Lineage Differentiation of Neural Stem Cells, and for Neuronal Incorporation into the Adult Olfactory Bulb

Gloria G. Curto,[1] Vanesa Nieto-Estévez,[2,3] Anahí Hurtado-Chong,[2] Jorge Valero,[1,4] Carmela Gómez,[1] José R. Alonso,[1,5,*] Eduardo Weruaga,[1,*] and Carlos Vicario-Abejón[2,3,*]

The paired type homeobox 6 (Pax6) transcription factor (TF) regulates multiple aspects of neural stem cell (NSC) and neuron development in the embryonic central nervous system. However, less is known about the role of Pax6 in the maintenance and differentiation of adult NSCs and in adult neurogenesis. Using the $+/Sey^{Dey}$ mouse, we have analyzed how *Pax6* heterozygosis influences the self-renewal and proliferation of adult olfactory bulb stem cells (aOBSCs). In addition, we assessed its influence on neural differentiation, neuronal incorporation, and cell death in the adult OB, both in vivo and in vitro. Our results indicate that the *Pax6* mutation alters $Nestin^+$-cell proliferation in vivo, as well as self-renewal, proliferation, and survival of aOBSCs in vitro although a subpopulation of $+/Sey^{Dey}$ progenitors is able to expand partially similar to wild-type progenitors. This mutation also impairs aOBSC differentiation into neurons and oligodendrocytes, whereas it increases cell death while preserving astrocyte survival and differentiation. Furthermore, Pax6 heterozygosis causes a reduction in the variety of neurochemical interneuron subtypes generated from aOBSCs in vitro and in the incorporation of newly generated neurons into the OB in vivo. Our findings support an important role of Pax6 in the maintenance of aOBSCs by regulating cell death, self-renewal, and cell fate, as well as in neuronal incorporation into the adult OB. They also suggest that deregulation of the cell cycle machinery and TF expression in aOBSCs which are deficient in Pax6 may be at the origin of the phenotypes observed in this adult NSC population.

Introduction

Adult neural stem cells (NSCs) located in the forebrain subventricular zone (SVZ) produce neuroblasts that migrate to the olfactory bulb (OB). Once in the OB, these neuroblasts differentiate into several neurochemical interneuron subtypes of granule and juxtaglomerular neurons [1–3]. Additional sources of interneurons may include the elbow of the rostral migratory stream (RMS) and the OB itself [4–11]. Adult neurogenesis is tightly regulated by both cell extrinsic and intrinsic mechanisms, among which transcription factors (TFs) play a major role, participating in several aspects of NSC maintenance, fate choice, and neuronal differentiation [12].

The paired type homeobox 6 (Pax6) TF exerts a pivotal role in brain patterning [13], embryonic cortical neurogenesis, and the formation of the olfactory system [14,15]. In fact, in *Pax6* homozygous mutant mice, an ectopic OB-like structure is formed [16,17]; whereas in humans, heterozygous mutations in *Pax6* result in forebrain abnormalities [18]. In addition to these functions in brain patterning, Pax6 regulates the proliferation, self-renewal, differentiation, and apoptosis of embryonic NSCs and progenitor cells in multiple brain regions [19–27]. However, a few studies have evaluated the role of this TF in the maintenance and cell fate of NSCs from the adult SVZ and hippocampus [28–30], and no studies have yet been published on the putative role of Pax6 in NSCs isolated from the adult OB [12].

In the adult mouse, Pax6 is expressed by numerous subpopulations of OB interneurons [14,31–33] and by different cell types in the SVZ-RMS region, including NSCs and neuroblasts [6,34,35]. Pax6 has been implicated in the specification and survival of dopaminergic periglomerular (PG) neurons, and in the differentiation and/or maintenance

[1]Instituto de Neurociencias de Castilla y León (INCyL), Universidad de Salamanca, Salamanca, Spain.
[2]Instituto Cajal, Consejo Superior de Investigaciones Científicas (CSIC), Madrid, Spain.
[3]Centro de Investigación Biomédica en Red Sobre Enfermedades Neurodegenerativas (CIBERNED), Madrid, Spain.
[4]Center for Neuroscience and Cell Biology (CNC), University of Coimbra, Coimbra, Portugal.
[5]Centro de Alta Investigación, Universidad de Tarapacá, Tarapacá, Chile.
*These authors contributed equally to this work.

of superficial granule cells, and of neurons expressing parvalbumin or calretinin (CR) in the external plexiform layer (EPL) [6,32,35–38]. Pax6 overexpression in progenitor cells induces neuronal differentiation [6,19,39–41] and results in an increase in the number of dopaminergic PG neurons [6], which is evidence that this TF exerts a neurogenic role. Furthermore, Pax6 has been proposed to act as a general neuronal determinant that might regulate the balance between neurogenesis and the formation of astrocytes or oligodendrocytes [20,22,29,42].

While *Pax6* homozygous mutants die shortly after birth, *Pax6* heterozygous mice are viable and mimic human heterozygous conditions [15,18,43]. Dickie's small eye (Sey^{Dey}) is an autosomic semidominant mutation affecting the *Pax6* gene and other proximal genes (the Wilms' tumor suppressor, *Wt1*, and reticulocalbin, *Rcn*, genes), although these latter two genes do not exert a relevant effect on the OB phenotype in heterozygotes [44–47]. We took advantage of this mouse model to analyze the effect of *Pax6* heterozygosis in the Sey^{Dey} mouse on the regulation of adult OB neurogenesis. The role of Pax6 in the regulation of aNSC self-renewal and proliferation, its influence on neural and neuronal subtype generation and differentiation, and on cell death in the adult OB was analyzed here, both in vivo and in vitro. Our results suggest that *Pax6* exerts a critical role in the maintenance and multi-lineage differentiation of aNSCs, and in the incorporation of newly formed neurons into the adult OB.

Materials and Methods

Animals

Adult heterozygous (+/Sey^{Dey}) and homozygous wild-type (+/+ o wt) male littermates (P75, P90, and P135) of the B6EiC3Sn-a/A-Pax6Sey^{Dey} mouse strain (Jackson ImmunoResearch Laboratories) were used in this study. Sey^{Dey} mice carry an autosomic and semidominant 1,370–2,300 kb deletion in chromosome 2 that affects the *Pax6* gene and its regulatory elements, as well as other proximal genes (*Wt1* and *Rcn*) [44–47]. The animals were maintained, handled, and sacrificed following the animal care rules of the Council of the European Communities (directives 86/609/EEC and 2010/63/EU) and Spanish legislation (RD 53/2013 and Law 32/2007), and the procedures were approved by the Bioethical Committee of both the University of Salamanca and the CSIC.

Bromodeoxyuridine injections and immunohistochemistry

To label proliferating cells and their progeny, we used intraperitoneal injections of the thymidine analog 5-bromo-2′-deoxyuridine (BrdU, 30 μg/g body weight; Sigma Chemical Co.), mixed with the thymidine synthesis inhibitor 5-fluoro-2′-deoxyuridine (FdU, 3 μg/g body weight; Sigma Chemical Co.) in 0.1 M phosphate-buffered saline (PBS), pH 7.3, as previously described [48]. Briefly, one dose of BrdU/FdU was injected intraperitoneally into P75 +/Sey^{Dey} and +/+ mice 30 min before sacrifice to quantify the proliferating cells in S-phase. To analyze the incorporation of newly generated cells into the OB and their survival, P75 mice were given three consecutive doses of BrdU every 3 h. These mice were then divided in two groups and were then sacrificed on P90 (15 days postinjection; 15 dpi) in order to study the arrival of neuroblasts to the OB and their differentiation into distinct neuronal subtypes, or at P135 (60 dpi) to analyze the survival of these cells.

For immunohistochemistry, mice were anesthetized with 5% chloral hydrate (10 μL/g), before they were perfused intraortically for 1 min with heparinized saline and for 15 min with a fixative solution containing 4% (w/v) paraformaldehyde (PFA) and 0.2% (w/v) picric acid in 0.1 M phosphate buffer (PB, pH 7.4). After perfusion, the rostral halves of the brain were dissected out and postfixed for 2 h in the same solution at room temperature (RT). The brain tissue was then washed in PB and cryoprotected with 30% (w/v) sucrose overnight at 4°C until they sank. The tissue was embedded in a mixture of 1.5% agar (w/v) and 5% sucrose (w/v) in PB and again cryoprotected in 30% sucrose. Coronal cryostat sections (30 μm) were then obtained, collected in PB, and stored at −20°C in a freezing mixture containing 30% (v/v) glycerol and 30% (v/v) polyethylene glycol in PB.

BrdU immunodetection alone or in combination with Nestin, Mash1, or Doublecortin (Dcx) immunodetection was carried out as previously described [48]. Briefly, sections were rinsed in PBS (3 × 10 min) and incubated for 1 h at 37°C with 2 N HCl to denature the DNA. The sections were then rinsed in 0.1 M borate buffer (pH 8.5) and PBS, and subsequently incubated for 48 h at 4°C with a rat anti-BrdU primary antibody (No. MAS250c; Accurate Chemical and Scientific Corporation) diluted 1:5,000 in PBS containing 0.2% Triton X-100 and 5% normal goat serum (Vector Laboratories) and with antibodies to detect Nestin (rabbit, 1:2,000; a gift from Dr. R. McKay, National Institutes of Health), Mash1 (mouse, 1:100; a gift from Dr. J. Johnson, UT Southwestern Medical Center), or Dcx (guinea pig, 1:3,000, No. AB2253; Millipore). The sections were then rinsed in PBS and incubated for 2 h at RT in either a biotinylated (1:1,000) or cyanin-conjugated anti-rat antibodies (1:500; Jackson ImmunoResearch Laboratories). Sections were washed in PBS and mounted immediately when a fluorescent secondary antibody was used or incubated for 2 h at RT with an avidin-biotin-peroxidase complex (Kit Elite ABC, 1:200; Vector Laboratories) when the biotinylated antibody was employed. Finally, these latter sections were rinsed thrice in PBS, twice in 0.1 M Tris-HCl buffer (pH 7.6), and the reaction product was visualized by exposing the sections to 0.02% 3,3′-diaminobenzidine (w/v) and 0.003% hydrogen peroxide (v/v) in 0.1 M Tris-HCl buffer (pH 7.6) until optimal staining intensity was achieved. Sections were dehydrated in increasing ethanol concentrations and mounted.

To analyze the phenotype of the newly generated neurons and to quantify the diverse neurochemical population densities, dual or simple immunofluorescence staining of sections was carried out as previously described [49,50] and using the following primary antibodies: rat anti-BrdU (1:5,000), rabbit anti-calbindin (CB, 1:8,000, No. CB-38; Swant), mouse anti-cholecystokinin (CCK, 1:200; Cure/Ria, University of California), rabbit anti-CR (1:10,000, No. 7699/3H; Swant), rabbit anti-tyrosine hydroxylase (TH, 1:10,000; Jacques Boy Institute), mouse anti-neuronal nuclear antigen (NeuN, 1:8,000, No. MAB377 clone A60; Millipore), sheep anti-nitric oxide synthase1 (NOS1, 1:10,000; K205) [51], and rabbit anti-Pax6 (1:1,000, No. PRB-278P; Covance). Cyanin-conjugated secondary antibodies (1:500; Jackson ImmunoResearch Laboratories) were used to visualize the primary antibody binding.

Cell nuclei were counterstained using either 4′,6-diamino-2-fenilindol (DAPI, 1:10,000, No. D9642; Sigma Chemical Co.) or propidium iodide (PI, 1:2,000, No. 81845; Sigma Chemical Co.) diluted in PBS. Finally, the sections were examined under an Olympus Provis AX70 microscope equipped with epifluorescence and the appropriate filter sets, and by confocal microscopy (Leica TCS SP2).

To detect proliferating cell nuclear antigen (PCNA) in proliferating cells, sections were postfixed for 2 h in Bouin 4% fixative (4% w/v PFA, 1% w/v picric acid, and 5% v/v acetic acid in PB) and then rinsed in PB (5 × 10 min). The sections were then incubated with a mouse anti-PCNA antibody (1:3,000, No. sc-56, clone PC10; Santa Cruz Biotechnologies), which was visualized with a cyanin-conjugated secondary antibody and mounted.

NSC culture

Adult olfactory bulb stem cells (aOBSCs) were prepared from OBs dissected out of P75 +/Sey^{Dey} and +/+ littermate mice as previously described [5,9]. The OBs were digested with papain and disaggregated, and the cell suspension was plated in uncoated six-well plates in Dulbecco's modified Eagle's medium (DMEM) with F12 and N2 supplements (Invitrogen), plus E13.5 OBSC conditioned medium (1:1), and in the presence of fibroblast growth factor-2 (FGF-2, 20 ng/mL; PeproTech) and epidermal growth factor (EGF, 20 ng/mL; PeproTech). When the cells reached confluence, the neurospheres were dissociated and re-plated in the same medium.

Proliferation assays were performed on neurospheres grown in the presence of FGF-2 and EGF for 4 and 7 days in vitro (DIV). BrdU (5 μM) was added to the culture medium for 1 h, and the neurospheres were collected in Matrigel and fixed in 4% PFA. To determine the capacity of aOBSCs to differentiate into neurons, astrocytes, and oligodendrocytes, cells from control and mutant mice were disaggregated and seeded at the same density in the absence of mitogens before they were fixed with 4% PFA after 1, 2, and 4 DIV. To analyze the neuronal subtypes, aOBSCs were plated and cultured for 7 days in a medium composed of DMEM/F12/N2/B27 with 2% fetal bovine serum (FBS) and a single dose of FGF-2 (20 ng/mL) [9]. Clonal analysis of aOBSC neurospheres was performed as previously described [52]. Briefly, 1 day after seeding, the wells containing a single cell were marked and induced to proliferate for 8 days, when the wells were screened for the presence of clonal neurospheres and fixed. Alternatively, the clonal neurospheres were disaggregated and then plated to form secondary spheres.

Immunostaining of cultured cells

Cells were fixed in 4% PFA for 30 min, incubated with 0.2% Triton X-100 and 5% serum for 30 min. and then with a primary rabbit antiserum against Tubulin β3 (TuJ1, 1:1,000, No. PRB-435P; Covance), mouse anti-GFAP (1:2,000, No. G3893, clone G-A-5; Sigma-Aldrich), mouse IgM anti-O4 (1:6; obtained from the culture media of O4-producing cells that were kindly provided by Dr. Rodríguez-Peña, CSIC), rabbit anti-S100β (1:2,000, No. 37; Swant), sheep anti-NOS1, rabbit anti-TH, rabbit anti-CB, mouse anti-CCK, rabbit anti-CR, and rat anti-BrdU. The antibody dilutions and the following steps were similar to those described earlier for immunohistochemistry except that the incubation times were reduced.

TUNEL assay

To detect apoptotic bodies, cells plated in proliferative and differentiation conditions were fixed with 4% PFA in PB for 20 min, rinsed in PBS, and treated with ethanol/acetic acid (2:1) at 20°C for 5 min. The cells were then washed with PBS and permeated at RT for 15 min with 0.2% Triton X-100 diluted in 0.1% sodium citrate (w/v). After permeation, dUTP nick end labeling (TUNEL) assays were carried out as previously described [48]. Briefly, cells were rinsed in PBS and immersed for 30 min in TUNEL buffer: 30 mM Tris-HCl buffer (pH 7.2) 140 mM sodium cacodylate, 1 mM cobalt chloride, and 0.3% Triton X-100. The cells were then incubated for 2 h at 37°C in the TUNEL reaction mixture containing 800 U/mL of terminal transferase (Roche Diagnostics) and 1 M biotin-16-2′-deoxy-uridine-5′-triphosphate (Roche Diagnostics), both of which were diluted in TUNEL buffer. Finally, the cells were washed with PBS, incubated at RT in the dark with Cy2-conjugated streptavidin (1:500; Jackson ImmunoResearch Laboratories), and counterstained with 1:2,000 PI.

RNA isolation and cDNA synthesis

Total RNA was extracted from wt and +/Sey^{Dey} aOBSCs using Trizol reagent (Invitrogen) and purified with Qiagen RNeasy Mini Kit separation columns (Qiagen). The reverse transcription reaction was carried out with SuperScript III (Invitrogen) to synthesize cDNA from the mRNA.

Real-time quantitative reverse transcription–polymerase chain reaction

The sequences of primer pairs for the quantitative polymerase chain reaction (qPCR) were designed with Lasergene software and are listed in Table 1. All PCR cDNA products obtained were sequenced and correspond to the expected fragments. The dynamic range of amplification for each primer set was determined using serial dilutions of cDNA. Finally, an optimal cDNA amount, which was within the dynamic range of the primer sets, was selected for the PCR reactions. A real-time qPCR analysis was performed in triplicate with the appropriate controls using Power SYBR Green (Applied Biosystems). The Ct value obtained for each target gene was normalized to the Ct value for *Gapdh* using the comparative CT method. Then, gene expression changes in the +/Sey^{Dey} aOBSCs were compared with the levels of gene expression obtained in the controls (wt), using the CT method and were expressed as fold changes in log2 scale [53].

Western blotting

Western blotting was performed as previously described [33] on extracts from +/Sey^{Dey} and +/+ neurosphere cultures taken on 4 and 7 DIV, and from differentiating cultures at 4 DIV. The membranes were probed with the following primary antibodies diluted in 5% nonfat milk and 0.1% Tween 20 in PBS: goat anti-Akt (1:1,000, No. 9272; Cell Signalling), rabbit anti-phospho-Akt^{Ser473} (p-Akt^{Ser473}, 1:1,000, No. 9271; Cell Signalling), mouse anti-phospho-p44/p42 MAP

Table 1. Primers Used for the Gene Profile Analysis of Adult Olfactory Bulb Stem Cells by RT-qPCR

Gene		*Primer (5′-3′)*	*Size (bp)*
Egfr	Forward	GGTGCTGTAACAGAGGACAACATAGAT	119
	Reverse	GGCTGATTGTGATAGACAGGGTTC	
Fgfr-1	Forward	CAGTGCCCTCTCAGAGACCTACG	188
	Reverse	TAACGGCTCATGAGAGAAGACAGA	
Fgfr-2	Forward	CGAAGACTTGGATCGAATTCTGACTC	107
	Reverse	AAGAGCTCCTTGTGTCGGGGTAAC	
Gapdh	Forward	GGTGAAGGTCGGTGTGAACG	233
	Reverse	CTCGCTCCTGGAAGATGGTG	
Gsx2	Forward	AGGAGAGAAGGGGACTCAGC	186
	Reverse	CGGACACTGACATCACCAAC	
Hes1	Forward	AGGCAGACATTCTGGAAATGA	183
	Reverse	TGATCTGGGTCATGCAGTTG	
Hes5	Forward	CACCAGCCCAACTCCAAG	218
	Reverse	TAGCCCTCGCTGTAGTCCTG	
Nestin	Forward	TGAGAACTCTCGCTTGCAGACACCT	298
	Reverse	CTGGGCTCTGACCTCTGCATTTTTAG	
Pax6	Forward	CAGCAGCAGCTTCAGTACCAGTGTCTA	259
	Reverse	GGTGTAGGTATCATAACTCCGCCCATT	
Rcn1	Forward	AAGCTGGACAAGGATGAGATTCGC	126
	Reverse	CTCCTCCTTGGTCAGCATCTCGTC	
Sox2	Forward	AGGGTTCTTGCTGGGTTTTGATTCT	137
	Reverse	CGGTCTTGCCAGTACTTGCTCTCA	
Wt1	Forward	CAACCACGGCACAGGGTATGAGA	156
	Reverse	GTTTCAGATGCTGACCGGACAAGAG	

The size (in base pairs, bp) of the PCR products is given and corresponds to fragments having the expected sequences.
RT-qPCR, real-time quantitative reverse transcription–polymerase chain reaction.

Kinase$^{(Thr202/Tyr204)}$ (hereafter referred to as p-Erk1/2; 1:2,000, No. 9101S; Cell Signalling), mouse anti-GAPDH (1 μg/mL, No. AM4300; Ambion), goat anti-p21$^{Waf/Cip1}$ (1:1,000, No. sc-397g; Santa Cruz Biotechnology), rabbit anti-p27^{Kip1} (1:1,000, No. sc-528; Santa Cruz Biotechnology), rabbit anti-p53 total (1:1,000, No. sc-6243; Santa Cruz Biotechnology), and goat anti-PTEN (1:1,000, No. sc-6818; Santa Cruz Biotechnology). Membranes were then incubated with peroxidase-conjugated secondary antibodies, and the signals from the labeled proteins were visualized by chemoluminescence (western-blotting luminol reagent; Santa Cruz Biotechnology), exposed to film, scanned, and digital images of the specific bands were imported and quantified using ImageJ software (Wayne Rasband, National Institutes of Health). The intensities of the bands were then compared according to their gray scale and corrected in function of the intensity of the GAPDH band to estimate the relative protein levels. A two-tailed Student's *t*-test was used to compare the mean values, and the differences in the two means were considered significant when $*P < 0.05$.

Quantitative and statistical analysis of sections and cultured cells

Equivalent serial coronal sections from +/Sey^{Dey} and +/+ mice were quantified considering anatomical landmarks and their relative positions to Bregma (Supplementary Fig. S1; Supplementary Data are available online at www.liebertpub.com/scd). PCNA$^+$ proliferative cells and the total number of cells (stained with PI) were quantified in SVZ coronal sections at five different rostrocaudal levels and in three quadrants (dorsal, lateral, and ventral) at each level. The proportion of PCNA$^+$ cells was estimated by counting the total number of cells and the number of PCNA$^+$ cells in a single plane of confocal microscopy images (Leica TCS SP2).

BrdU$^+$ cells were quantified, and the areas and volumes of the layers were estimated using Neurolucida software (MicroBrightField) as previously described [48]. The areas of the different regions of interest and the total area of the section were measured in serial sections (30 μm) at 180 μm rostrocaudal intervals. The volume of the layers was calculated using Table-Curve 2D v5.01 (AISN Software). The density of BrdU$^+$ cells was calculated and the total number of BrdU$^+$ cells in each region or layer was corrected by an Abercrombie-based method, as previously reported [48,54], applying the formula $N=(d*V)/(t+D)$ (N, total number of BrdU$^+$ estimated in a given volume, V; d, density of BrdU$^+$ cells, t, thickness of the sections and D, mean diameter of the particles analyzed).

Equivalent SVZ or OB sections were chosen from +/Sey^{Dey} and +/+ mice to determine the percentage of BrdU$^+$ cells expressing Nestin, Mash1, Dcx, or different neuronal markers. A confocal plane from the dorsal, lateral, ventral, and medial OB quadrants was analyzed using the Leica confocal software (v2.61) and ImageJ 1.37i software. Cell densities in +/Sey^{Dey} were corrected by applying a coefficient related to the +/Sey^{Dey} OB volume loss as previously described [50].

The diameter of +/Sey^{Dey} and +/+ neurospheres growing from 2 to 7 DIV was measured using Image J software. To calculate the proportions of the different cell populations in culture, the mean value of the cells counted in 10 random fields on a coverslip were considered, and at least three cultures were quantified per condition.

For statistical analyses, the PASW Statistics 18 (SPSS) and GraphPad Prism software programs were used. A two-tailed Student's *t*-test was used to compare the parametric

values. In cases where the variances differed, the data were analyzed using the Mann–Whitney *U* two-group comparisons. The differences between groups were considered statistically significant when $P < 0.05$.

Results

Defects in proliferation and self-renewal in cells from adult +/Sey^{Dey} mice, both in vivo and in vitro

Pax6, one of the genes deleted in the +/Sey^{Dey} mutation [44–46], is known to regulate the proliferation of NSCs and progenitor cells during embryonic brain development [19,21,55–58]. Here, we have studied the impact of Pax6 heterozygosis on NSC maintenance and differentiation in the adult OB and SVZ.

First, coronal SVZ sections from +/+ and +/Sey^{Dey} P90 mice were immunostained with anti-PCNA to detect proliferating cells (Fig. 1A), and quantifying the total number of (PI stained) cells (Fig. 1B), to calculate the proportion of proliferative cells (%PCNA$^+$; Fig. 1C). Given the morphological modifications and distinct volumes between adult +/+ and +/Sey^{Dey} brains, these parameters were quantified in anatomically comparable and equidistant regions (Supplementary Fig. S1). There were 31% more PI$^+$ cells in the +/Sey^{Dey} than the +/+ mice ($P < 0.01$), whereas there were fewer proliferative PCNA$^+$ cells, although only in the ventral quadrant of the rostral-most level of the SVZ of +/Sey^{Dey} adult mice. Indeed, compared with controls, the proportion of proliferating cells was 3.6-fold lower in +/Sey^{Dey} mice in this region (Fig. 1A–C; $P < 0.01$). Three different proliferative cell types can be distinguished in the adult SVZ in vivo: NSCs, transit amplifying progenitors, and neuroblasts. They can be recognized through their expression of Nestin, Mash1, and Dcx, respectively [33,59]. To analyze the impact of the +/Sey^{Dey} mutation on the proliferation of these three cell types, we determined the percentage of cells expressing Nestin, Mash1, or Dcx that incorporated BrdU 30 min after its injection. The proportion of BrdU 30 min Nestin$^+$ cells decreased in heterozygous mice compared with the wild type (+/+, 24.06% ± 1.66%; +/Sey^{Dey}, 18.20% ± 1.68% Nestin$^+$-BrdU$^+$/BrdU$^+$ cells: $P < 0.05$; Fig. 1D, E). By contrast, there was no significant difference in the percentage of BrdU 30 min Mash1$^+$ cells (+/+, 28.65% ± 2.11%; +/Sey^{Dey}, 31.96% ± 1.88% Mash1$^+$-BrdU$^+$/BrdU$^+$ cells: $P = 0.254$), nor in that of Dcx$^+$ neuroblasts (+/+, 18.5% ± 2.12%; +/Sey^{Dey}, 22.21% ± 1.9% Dcx$^+$-BrdU$^+$/BrdU$^+$ cells: $P = 0.205$; Fig. 1F, G). These results indicate that Pax6 heterozygosis in the +/Sey^{Dey} mouse has a specific effect in reducing the proliferation of aNSCs in vivo.

Since the +/Sey^{Dey} brain has a smaller OB than the wt brain, we estimated the total number of proliferative cells in this brain region, as well as in the SVZ and RMS (that supply the OB with cells), using an Abercrombie-based method. We first injected P75 adult mice with BrdU at 30 min before sacrifice in order to label S-phase proliferating cells. We quantified the cell densities and tissue areas along the rostro-caudal axis (Supplementary Fig. S1), and we estimated the total number of S-phase proliferative cells in the whole SVZ-RMS-OB region. The total number of BrdU$^+$ cells estimated in this region was significantly lower in +/Sey^{Dey} mice than in the +/+ mice (+/Sey^{Dey}, 7,907.6 ± 656.5 cells; +/+, 11,003.0 ± 464 cells: $P < 0.05$). Moreover, their distribution was altered in the different subregions (SVZ, RMS, and OB). Indeed, the number of BrdU$^+$ cells in the SVZ of +/Sey^{Dey} mice was significantly reduced by 30% (Fig. 1H; $P < 0.05$). The values for the OB were +/Sey^{Dey}, 1,621.0 ± 302.8 BrdU$^+$ cells; +/+, 2,678.0 ± 275.8 BrdU$^+$ cells: $P = 0.0508$; nonstatistically significant (Fig. 1I). Next, the number of BrdU$^+$ cells was analyzed in greater detail at five equally spaced rostrocaudal levels of the SVZ. The density of BrdU$^+$ cells was significantly different in the two rostral-most levels (SVZ-MR +/+, 1,529.29 ± 62.87 cells/mm^2; +/Sey^{Dey}, 1,282.85 ± 53.69 cells/mm^2 and SVZ-R +/+, 1,863.17 ± 195.79 cells/mm^2; +/Sey^{Dey}, 587.10 ± 488.18S cells/mm^2: $P < 0.05$). Altogether, these results indicate that the proliferation rate in the most rostral regions of the SVZ was lower in +/Sey^{Dey} mice, specifically affecting the population of Nestin$^+$ cells.

The findings mentioned earlier encouraged us to analyze the proliferative capacity of aOBSCs in vitro [9]. The neurospheres formed in aOBSC cultures prepared from P75 to P90 +/Sey^{Dey} and +/+ mice were analyzed after a 1 h BrdU pulse, and the PI and BrdU$^+$ cells were quantified in confocal planes (Fig. 1J). Compared with those from +/+ mice, +/Sey^{Dey} neurospheres were smaller in size and contained significantly fewer PI$^+$ and BrdU$^+$ cells at all DIV analyzed (Fig. 1K). The proportion of BrdU$^+$ cells was also significantly lower in the +/Sey^{Dey} spheres at 2 (62%; $P < 0.01$) and 4 DIV (39%; $P < 0.01$), but it was higher than in the +/+ neurospheres at 7 DIV (50%; $P < 0.01$) (Fig. 1L). These in vitro results indicate that +/Sey^{Dey} aOBSCs experience a deficit of proliferation, although a subpopulation of progenitors maintain the capacity to proliferate. They also suggest a possible effect of the mutation on aOBSC survival (see Results on Cell death). Together, both the in vivo and in vitro data indicate that the +/Sey^{Dey} mutation, and therefore *Pax6* haploinsufficency, alters (mainly negatively) progenitor cell proliferation in the adult SVZ and OB.

In order to understand how *Pax6* haploinsufficiency alters the growth of the neurospheres, aOBSCs were plated under population conditions at 5,000 cells/cm^2 (high density) (Fig. 2A, B), and the diameter of +/Sey^{Dey} and +/+ neurospheres was measured daily from DIV 2 to 7 (Fig. 2F), the day when +/+ neurospheres reached confluence. Neurospheres from +/Sey^{Dey} aOBSC cultures (Fig. 2B) had a smaller diameter than the +/+ spheres (Fig. 2A) on each day analyzed except at 7 DIV (Fig. 2F; $P < 0.01$). These results show the negative impact of the *Pax6* haploinsufficiency on the growth of the OBSC cultures. The absence of a significant difference in the size of the neurospheres at 7 DIV in this assay was probably due to wt cultures having reached confluence, stopping their growth, unlike the +/Sey^{Dey} cultures. To assess how the initial cell density influences the phenotype observed, cells were seeded at 2,500–3,000 cells/cm^2 (low density) and the sphere diameter was measured 6, 7, and 8 days later (Fig. 2G). When seeded at low density, the +/Sey^{Dey} cells gave rise to significantly smaller neurospheres than the wt cells, indicating that when plated at low density the slower proliferation of +/Sey^{Dey} aOBSCs is maintained throughout the duration of the culture.

To determine whether *Pax6* haploinsufficiency affects the self-renewal of aOBSCs, these cells were seeded under clonal conditions, seeding one cell per well (Fig. 2C–E, H), and the percentage of newly formed clonal neurospheres

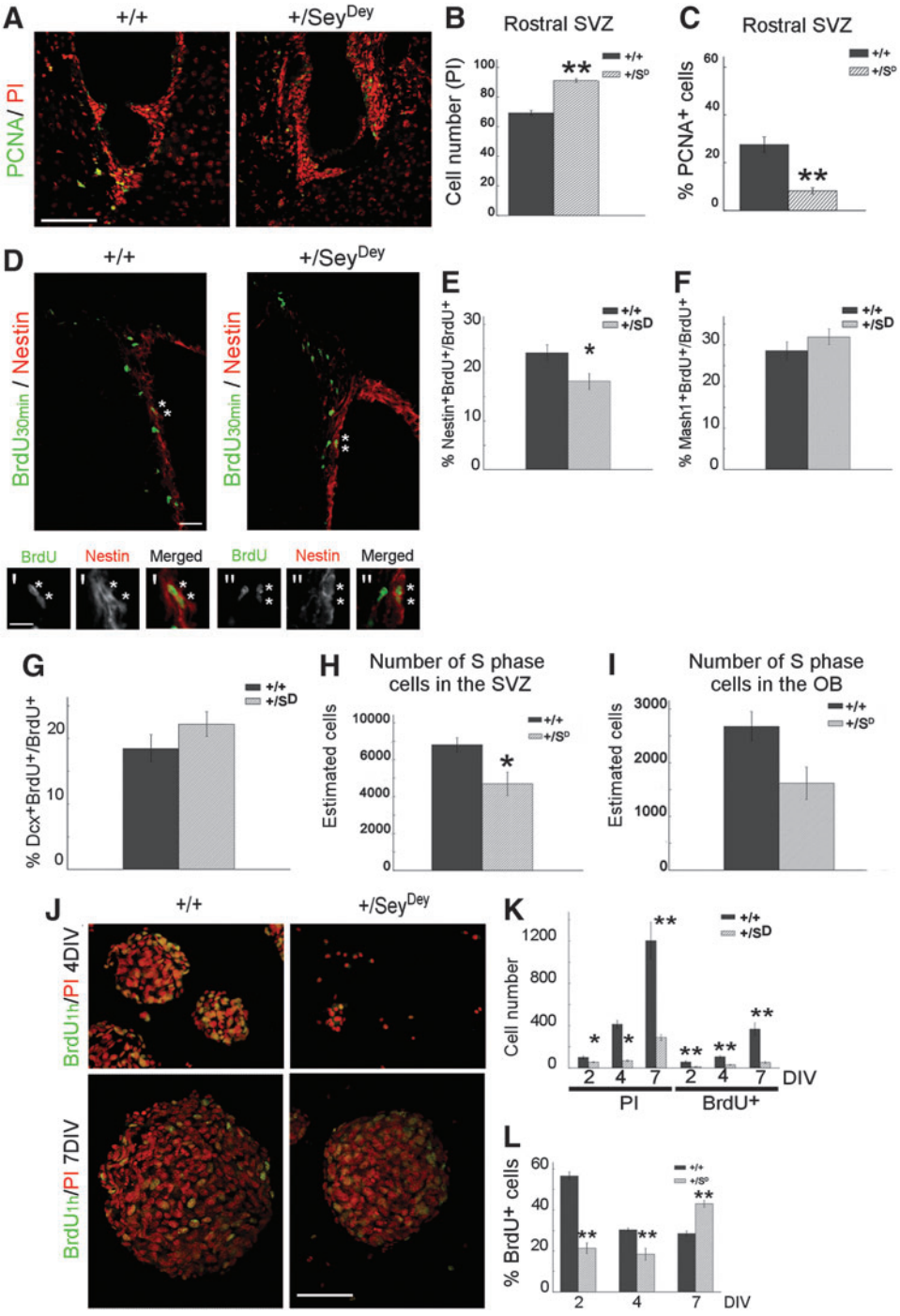

FIG. 1. Proliferation defects in the adult +/Sey^{Dey} mice. In the rostral region of the +/Sey^{Dey} subventricular zone (SVZ) **[A;** coronal sections; PCNA^{+}, *green*; propidium iodide (PI), *red*], the rate of cell proliferation is lower than in wild-type mice **(C),** whereas the total cell number is significantly higher in the +/Sey^{Dey} SVZ **(B)**. The percentage of Nestin^{+} (*red*) proliferative cells [5-bromo-2′-deoxyuridine (BrdU), *green*] is significantly reduced in +/Sey^{Dey} mouse SVZ compared with the wt **(D, E)**. The *insets* (′, ″) show details of Nestin^{+}-BrdU^{+} cells. The percentages of Mash1^{+} **(F)** and Doublecortin^{+} (Dcx^{+}, **G)** BrdU^{+} cells are similar in wt and +/Sey^{Dey} mice. The number of S phase cells (BrdU^{+} cells; 30 min after a single BrdU injection in p75 mice) is also significantly decreased in the +/Sey^{Dey} SVZ **(H),** whereas the reduction in the olfactory bulb (OB) is not statistically significant **(I)**. In vitro, adult OB-derived neurospheres from +/Sey^{Dey} P75 adult mice also show defects in proliferation compared with wt neurospheres **(J–L)**. The total number of cells (PI, *red*) diminishes severely at 2, 4, and 7 days in vitro (DIV) in the +/Sey^{Dey} cultures **(J;** quantified in **K)**, as does the number of proliferative cells (BrdU^{+}, *green*) when compared with the wild type **(J;** quantified in **L)**. The percentage of BrdU^{+} cells in the +/Sey^{Dey} cultures is significantly lower at 2 and 4 DIV, while it increases at 7 DIV, even considering that +/Sey^{Dey} cultures at 7 DIV have lower total and proliferative cell numbers compared with the +/+ cultures **(K)**. Results represent the mean ± SEM from three animals per genotype and from at least three cultures per condition. Scale bars: **(A, J)** 50 μm; **(D)** 32.3 μm; **(D′, D″)** 16.15 μm.*$P < 0.05$; **$P < 0.01$.

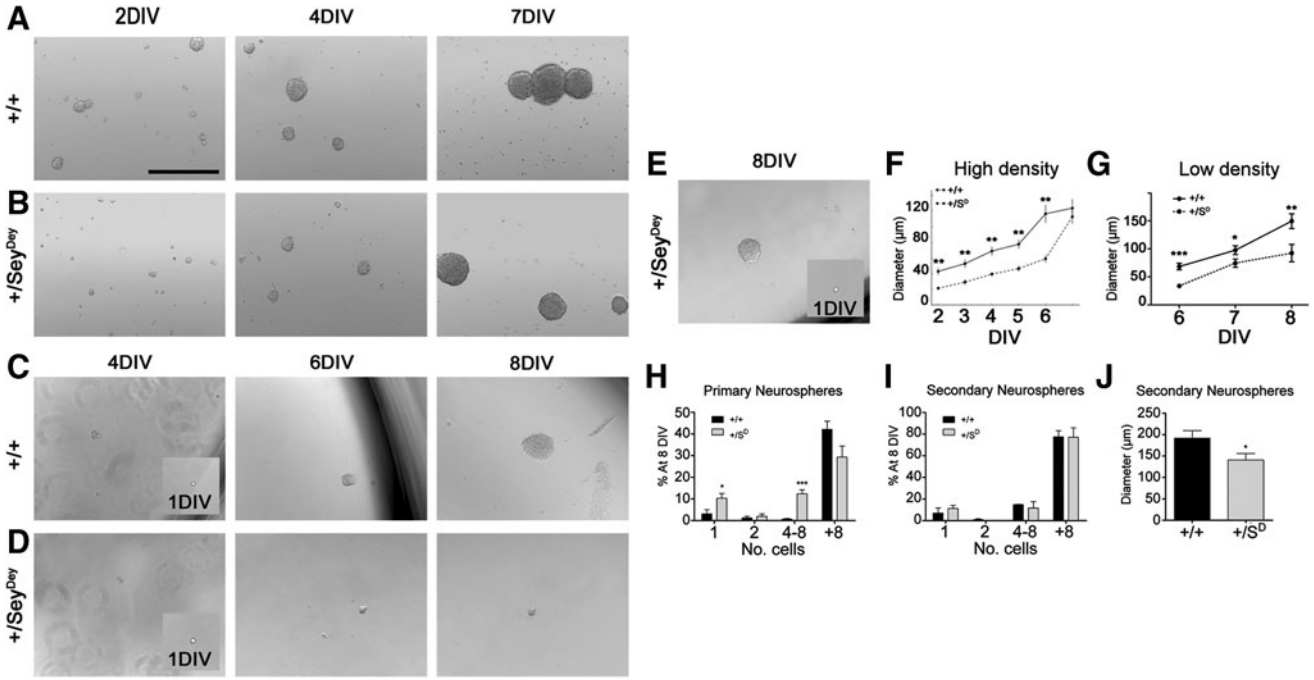

FIG. 2. The self-renewal of aOBSCs is altered in +/Sey^{Dey} cultures. Images of wild-type **(A)** and +/Sey^{Dey} **(B)** p75 adult mice aOBSC cultures at 2, 4, and 7 DIV, maintained under population conditions. It should be noted that +/Sey^{Dey} neurospheres at 2 and 4 DIV **(B)** are smaller than the wild-type spheres **(A)**. **(F, G)** Quantification of the diameter (µm) of these nonclonal neurospheres at different days shows that +/Sey^{Dey} neurospheres are smaller than the wild-type spheres, except for the day on which the +/+ spheres reach confluence (7 DIV), when the cells are plated at high density **(F)**. However, when the cells are plated at low density **(G),** the +/Sey^{Dey} neurospheres are smaller than the wild-type spheres at all the time points analyzed. **(C–E)** Wild-type **(C)** and +/Sey^{Dey} **(D, E)** neurospheres were dissociated and plated under clonal analysis conditions, and only wells containing a single cell were analyzed. Images illustrate single cells at 1, 4, 6, and 8 DIV. **(H)** Quantification of clonal division of single cells after 8 DIV ($n=6$ cultures per condition). The +/Sey^{Dey} single cells generated more clusters composed of less than eight cells and they also remained as single cells more frequently than wt cells **(D)**, indicating alterations in self-renewal. When the primary neurospheres were seeded, the percentages of cells that formed secondary neurospheres or gave rise to four to eight cell clusters or remained as single cells at 8 DIV were similar in +/Sey^{Dey} and wt cultures **(I)**. However, mutant secondary neurospheres ($n=31$) have a significantly lower size than the wt ones ($n=35$) **(J)**. Results represent the mean ± SEM from six cultures per condition (primary clonal analysis) and from two cultures (secondary clonal analysis). Scale bar: 300 µm. *$P<0.05$, **$P<0.01$, and ***$P<0.001$.

(composed of more than eight cells) [52] was measured at 8 DIV. In addition, the proportion of cells that remained as single cells, duplets, or groups of four to eight cells was also determined after 8 DIV. The number of wells containing one single cell the day after seeding was similar in cultures from both genotypes (wt: 41.0 ± 6.8; +/Sey^{Dey}: 44.5 ± 4.2; $n=6$), and a 42.7% ± 4.7% and 54.2% ± 2.6% of the single cells in the wt and mutant cultures, respectively, were able to survive for 8 days and generate clones or remain as single cells. There were no statistically significant differences ($P=0.06$) in the proportion of +/Sey^{Dey} (29.3 ± 5.0) or +/+ neurospheres (42.1% ± 3.7%) generated from single cells (Fig. 2E, H), and the clonal neurospheres generated from +/Sey^{Dey} single cells had similar diameters to those from the wt cells (+/+, 74.32 ± 6.27 µm, $n=23$; +/Sey^{Dey}, 75.22 ± 5.64 µm, $n=20$: $P=0.916$). However, there was a significant increase in the proportion of +/Sey^{Dey} single cells that gave rise to four to eight cell clusters and cells which remained as single cells at 8 DIV (Fig. 2C, D, H; $P<0.05$ and $P<0.001$). These findings suggest that subpopulations of +/Sey^{Dey} cells divide only a limited number of times or not at all, remaining as single cells. When the primary neurospheres were seeded, the percentages of cells that formed secondary neurospheres or gave rise to four to eight cell clusters or remained as single cells at 8 DIV were similar in +/Sey^{Dey} and wt cultures. However, the size of mutant secondary neurospheres was significantly lower than that of wt ones (Fig. 2J; 26%, $P<0.05$). All these results suggest a role for Pax6 in the regulation of aOBSC self-renewal and proliferation. They also show that some +/Sey^{Dey} cells may be able to expand partially similar to wild-type progenitors.

To explore the molecular mechanisms associated to the +Sey^{Dey} mutation, the expression of TFs involved in the regulation of self-renewal (*Sox2*, *Gsx2*, *Hes1*, and *Hes5*) [9,12,60,61] and cell proliferation, and that of markers of NSCs and progenitors (*Egfr*, *Fgf-1r*, *Fgf-2r*, and *Nestin*) [10] was measured in aOBSCs (Fig. 3). We first found that the level of *Pax6* mRNA was 2.6-fold lower (in log2 scale) in the +Sey^{Dey} cells than in the control cells, whereas the expression of Wt1 was below the detection limit and that of the *Rcn* was similar in both these cell types. By contrast, *Gsx2* was upregulated (1.5-fold) in the +Sey^{Dey} cells; whereas the expression of *Sox2*, *Hes1*, *Hes5*, *Egfr*, and *Nestin*, and of *Fgfr-1* and *Fgfr-2* (data not shown) remained unaffected or was only marginally affected by the mutation (Fig. 3). All these results suggest that downregulation of *Pax6* and

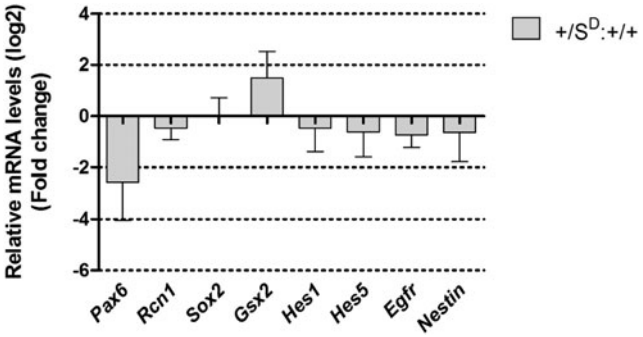

FIG. 3. Gene expression in aOBSCs from +/Sey^{Dey} and wild-type mice. RNA was extracted from aOBSCs and transcribed to cDNA, and the expression of genes affected in the +/Sey^{Dey} mutation, genes involved in self-renewal or cell proliferation, as well as that of *Nestin*, was quantified by real-time quantitative polymerase chain reaction. The graphs show that in mutant aOBSCs there was a 2.6-fold decrease in paired type homeobox 6 (*Pax6*) and a concomitant increase in *Gsx2* mRNA expression. No changes or only minor changes were observed in the other transcripts analyzed. The results are the mean ± SEM of four experiments performed in triplicate.

upregulation of *Gsx2* may be involved in the altered self-renewal produced by the +/Sey^{Dey} mutation in OBSCs.

Multi-lineage differentiation of aOBSCs is altered in +/Sey^{Dey} progenitors

Although it was previously shown that Pax6 is involved in the generation of different types of neurons in the adult OB, the role of Pax6 in the differentiation of aOBSCs into neurons and glial cells has yet to be studied. To address this issue, we dissociated wild-type and +/Sey^{Dey} aOBSC neurospheres, plating the cells at the same density in the absence of mitogens (FGF-2 and EGF), and we quantified the number of TuJ1$^+$ (neurons), O4$^+$ (oligodendrocytes), and GFAP$^+$ cells (astrocytes) that developed after 1 and 2 DIV (Fig. 4, arrows). It is known that GFAP is a marker of aNSCs located in the SVZ and the SGZ [59]. However, we previously found $<1.5\%$ GFAP$^+$ cells in aOBSCs growing as neurospheres under exactly the same conditions used here (with a daily supply of FGF-2 and EGF). By contrast, when aOBSCs were plated under differentiation conditions, 50% of the cells in the cultures expressed GFAP [10].

These results indicate that the GFAP$^+$ cells derived from aOBSCs under our culture conditions are most probably astrocytes rather than NSCs. Nonetheless, we immunostained aOBSC cultures differentiated for 2 days with a rabbit antibody against S100β and while S100β$^+$ cells could not be found in these cultures, S100β$^+$ cells were clearly detected in cultures of embryonic OBSCs that differentiated over 14 days (data not shown). Thus, we used a GFAP antibody to label astrocytes in this study.

The generation and/or survival of TuJ1$^+$ cells was severely and rapidly impaired in +/Sey^{Dey} cultures compared with controls after 1 DIV (Fig. 4A, B, G; $P<0.05$). Similar results were obtained in 2 DIV cultures ($P<0.05$), although the proportion of TuJ1$^+$ neurons increased in both mutant and +/+ cultures between 1 and 2 DIV. The +/Sey^{Dey} mutation also produced a sharp reduction in the percentage

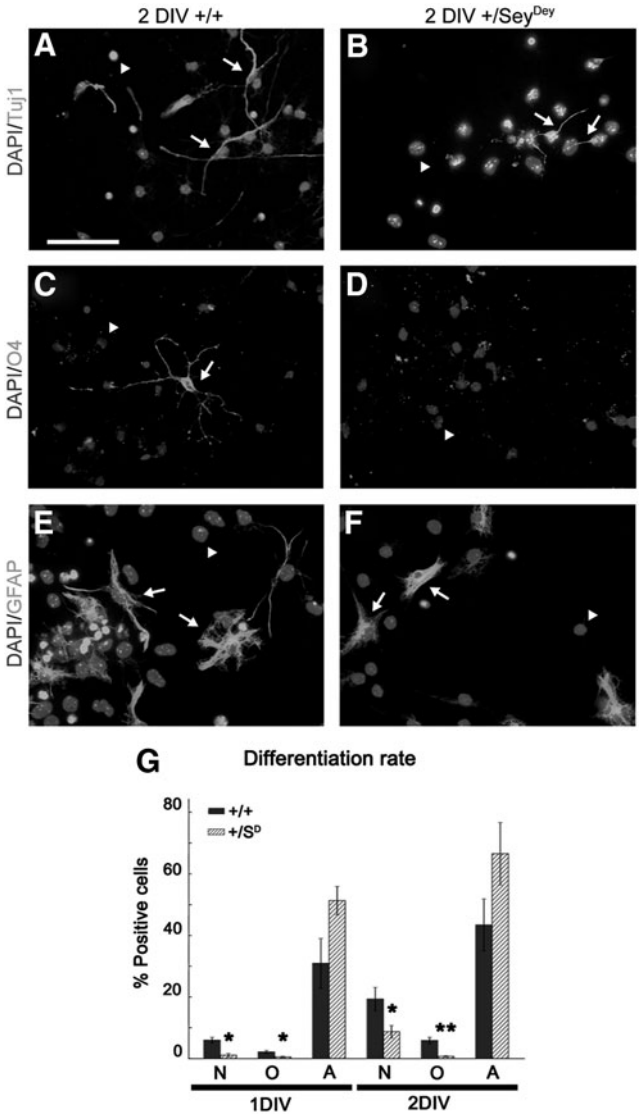

FIG. 4. aOBSC multi-lineage differentiation is compromised in the +/Sey^{Dey} cultures. Neurospheres from wild-type **(A, C, E)** and +/Sey^{Dey} **(B, D, F)** cultures were dissociated and plated at the same density in the absence of mitogens in order to analyze their differentiation capabilities: differentiation into neurons (TuJ1$^+$, *arrows*; **A, B**), oligodendrocytes (O4$^+$, *arrow*; **C, D),** and astrocytes (GFAP$^+$, *arrows*; **E, F**). The generation and/or survival of neurons and oligodendrocytes decreased at both 1 and 2 DIV in cultures of +/Sey^{Dey} aOBSC compared with the wild-type cultures **(G)**. No statistically significant differences were evident in the proportion of astrocytes **(G)**. *Arrowheads* point to DAPI nuclei. Results represent the mean ± SEM from at least three cultures per condition. Scale bar: 50 μm. $^*P<0.05$; $^{**}P<0.01$.

of O4$^+$ oligodendrocytes generated from aOBSCs at 1 ($P<0.05$) and 2 DIV ($P<0.001$; Fig. 4C, D, G), which were nearly absent from the cultures. By contrast, the generation and survival of astrocytes did not seem to be significantly affected (1 DIV, $P=0.083$; 2 DIV, $P=0.131$; Fig. 4E-G). These results suggest that Pax6 regulates the multi-lineage differentiation of aOBSCs in diverse and contrasting ways, promoting neurogenesis and oligodendrogenesis, while preserving astrocyte survival and differentiation.

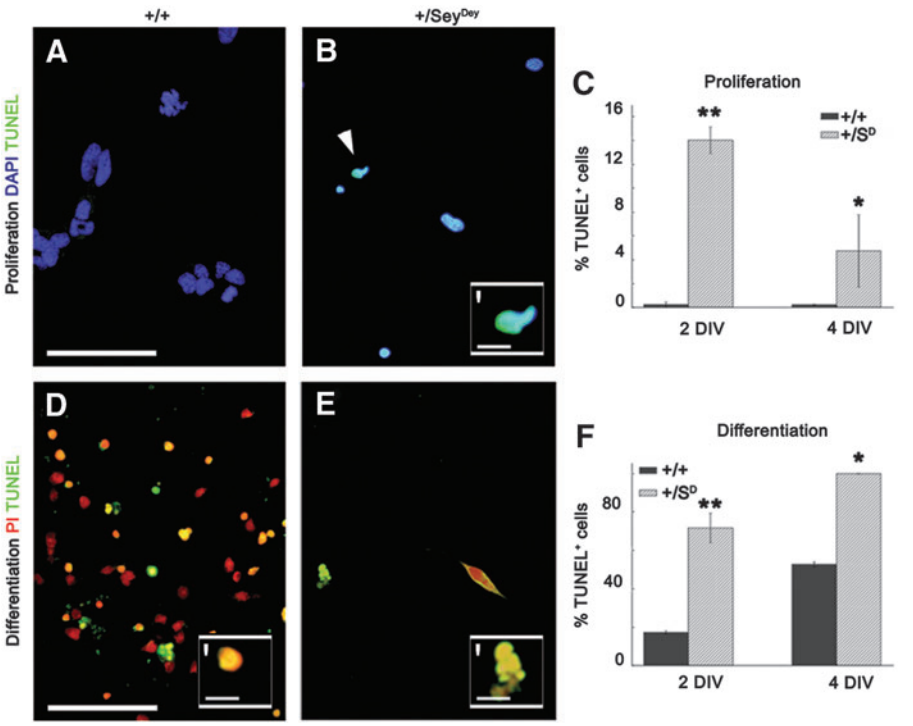

FIG. 5. Increased cell death in proliferating and differentiating +/Sey^{Dey} aOBSCs. A few dissociated proliferative cells derived from aOBSC neurospheres from wild-type cultures were TUNEL$^+$ at 2 DIV [dUTP nick end labeling (TUNEL); *green*; **A**], whereas TUNEL$^+$ cells were readily detected in +/Sey^{Dey} cultures **(B)**. **(C)** +/Sey^{Dey} aOBSC proliferative cultures displayed an increased rate of cell death, at both 2 and 4 DIV. **(D, E)** TUNEL staining (*green*) of differentiating cells at 4 DIV. The +/Sey^{Dey} cultures **(E)** have fewer cells than the wild-type cultures **(D)**, and TUNEL staining is evident in all of them at 4 DIV. **(F)** Cell death is increased at 2 DIV in the +/Sey^{Dey} cultures, and by the fourth day every cell that remains in the culture is dying (TUNEL$^+$). Results represent the mean ± SEM from at least three cultures per condition. Scale bars: **(A, B)** 25 μm; **(D, E)** 50 μm; **(B′)** 3.1 μm; **(D′, E′)** 6.2 μm. *P value <0.05; **P value <0.01.

Cell death is enhanced in +/Sey^{Dey} cultures growing under conditions of proliferation and differentiation

The maintenance of both proliferative and postmitotic cells requires the tight regulation of cell survival and cell death. To determine whether survival was affected in the +/Sey^{Dey} mutant cells, we evaluated cell death in proliferative aOBSC cultures at 2 and 4 DIV using a TUNEL assay (Fig. 5). As mentioned earlier (Fig. 1K), wild-type cultures contained more PI$^+$ cells than +/Sey^{Dey} cultures at both 2 and 4 DIV ($P<0.05$). By contrast, the percentages of TUNEL$^+$ cells were 63.7 and 21.5 times higher in the +/Sey^{Dey} proliferative aOBSC cultures than in the wild-type cultures at 2 DIV ($P<0.001$) and 4 DIV ($P<0.05$), in which TUNEL$^+$ cells were nearly absent (Fig. 5A–C). A similar pattern of cell death was observed in +/Sey^{Dey} aOBSC cultures growing under differentiation conditions after growth factor (FGF-2 and EGF) withdrawal (Fig. 5D–F), conditions that induce differentiation and enhance cell death. After 2 DIV, the percentage of TUNEL$^+$ cells increased 4-fold in +/Sey^{Dey} cultures compared with controls ($P<0.01$; Fig. 5F) and at 4 DIV, the total number of cells in +/Sey^{Dey} cultures was reduced dramatically compared with +/+ cultures (+/+, 488.67 ± 37.89 cells; +/Sey^{Dey}, 40.67 ± 1.86 cells: $P<0.05$; Fig. 5D–F) and the ratio of TUNEL$^+$ cells in +/Sey^{Dey} cultures reached 100% (Fig. 4D–F; $P<0.05$). These findings suggest that *Pax6* heterozygosis in the +/Sey^{Dey} mouse is lethal to aOBSCs during the early differentiation process in vitro, and that cells deficient in *Pax6* undergo an alteration in either cell cycle exit before differentiation or in the very early events of NSC differentiation after cell cycle exit.

Since cell survival, proliferation, and early differentiation is markedly impaired by Pax6, we evaluated the levels and phosphorylation status of different signaling molecules of the Akt and MAPK signaling pathways (Akt, p-Akt^{Ser473}, PTEN, and p-Erk1/2) that could regulate NSC maintenance and differentiation [62], and the expression of the cell cycle regulators p21$^{Waf1/Cip1}$, p27^{Kip1} (hereafter referred to as p21 and p27), as well as the p53 proteins which are known to exert an important influence on proliferation and survival of neural progenitor cells [63–65]. There were no significant changes in the levels of Akt, p-Akt^{Ser473}, PTEN, and P-Erk1/2 detected in cells growing under proliferation conditions (4 and 7 DIV) (Fig. 6A, B). By contrast, in proliferative cultures, the expression of cell cycle regulators p21, p27, and p53 was diminished at 4 DIV (Fig. 6C, D), suggesting a role for Pax6 in the regulation of molecular components of aOBSC cell cycle machinery. When we evaluated the expression of Akt, p-Akt^{Ser473}, PTEN, and P-Erk1/2 and the cell cycle regulator p27 in 2 DIV differentiating cultures, we were unable to detect significant changes in the expression or phosphorylation status for any of these molecules (Fig. 6E, F).

To evaluate the cell death that occurs in the neurogenic SVZ-RMS-OB region in vivo, we quantified the number of TUNEL$^+$ apoptotic bodies per section in every region of interest (Supplementary Fig. S1). A similar number of apoptotic bodies was detected in all the regions analyzed, except for an increase in the TUNEL$^+$ cells evident in the +/Sey^{Dey} RMS (+/+, 0.66 ± 0.36 cells/section; +/Sey^{Dey}, 1.25 ± 0.25 TUNEL$^+$ cells/section: $P<0.05$) and the reduced cell death in the OB glomerular layer (GL) of +/Sey^{Dey} mice (+/+, 0.78 ± 0.15 TUNEL$^+$ cells/coronal section; +/Sey^{Dey}, 0.26 ± 0.09 TUNEL$^+$ cells/coronal section: $P<0.05$).

Together, these in vivo and in vitro data support a role for Pax6 in regulating the balance between self-renewal and cell death, and in the early events of NSC differentiation in the adult brain.

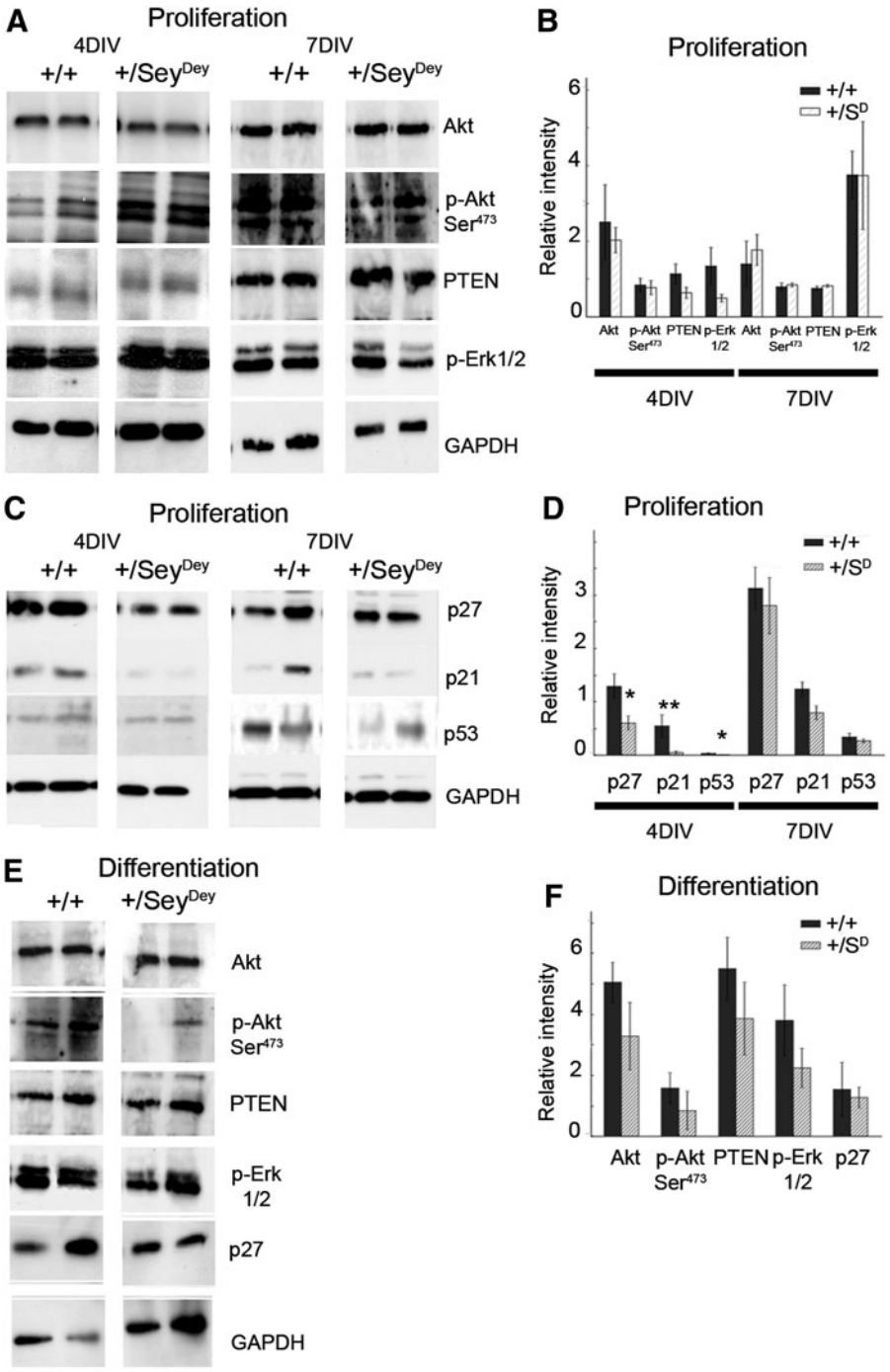

FIG. 6. Expression of cell signaling and cell cycle-related molecules in proliferative and differentiating aOBSCs. **(A)** Western blot detection of Akt, p-Akt^{Ser473}, PTEN, p-Erk1/2$^{(Thr202/Tyr204)}$, and GAPDH in aOBSCs after 4, and 7 DIV in proliferation conditions. The relative expression quantified by densitometry was similar in +/Sey^{Dey} cells and wild-type cells **(B)**. **(C)** Western blot analysis of p21, p27, and p53 in proliferative aOBSCs at 4 and 7 DIV. Quantification of the relative expression of these proteins **(D)** revealed a significant decrease in p21, p27, and p53 expression at 4 DIV. **(E)** Akt, p-Akt^{Ser473}, PTEN, p-Erk1/2$^{(Thr202/Tyr204)}$, and p27 in differentiating cells at 2 DIV do not demonstrate any differences in their relative levels of expression between both cultures **(F)**. Results represent the mean ± SEM from four to six cultures per condition. $^{*}P < 0.05$; $^{**}P < 0.01$.

Differentiation and survival of the main neurochemical types of OB interneurons is significantly impaired in +/Sey^{Dey} aOBSC cultures

Pax6 is thought to be necessary for the generation and/or the maintenance of various neuronal subtypes in the adult OB [6,32,35–38]. In this work, we wanted to analyze the capacity of *Pax6* heterozygous aOBSCs to differentiate into different neurochemical subtypes of interneurons (Fig. 7). To favor neuronal survival and differentiation-maturation, phenomena that were compromised by growth factor withdrawal in the mutant cells (Fig. 5F), we cultured dissociated neurosphere cells for 7 days in DMEM/F12/N2/B27 medium plus 2% FBS [9]. Cell survival was quantified in these conditions through the total number of DAPI cells at 7 DIV and on average, the cultures prepared from +/Sey^{Dey} mice had 28% fewer cells (281.2 ± 23.25) than the +/+ cultures (391.25 ± 21.64; $P < 0.01$). However, not statistically significant differences in the number of dead cells were detected by TUNEL staining at 7 DIV (+/+: 14.86% ± 2.16% TUNEL^{+} cells; +/Sey^{Dey}: 6.44% ± 0.52% TUNEL^{+}: $P = 0.215$). Since the total number of cells was lower in the +/Sey^{Dey} cultures,

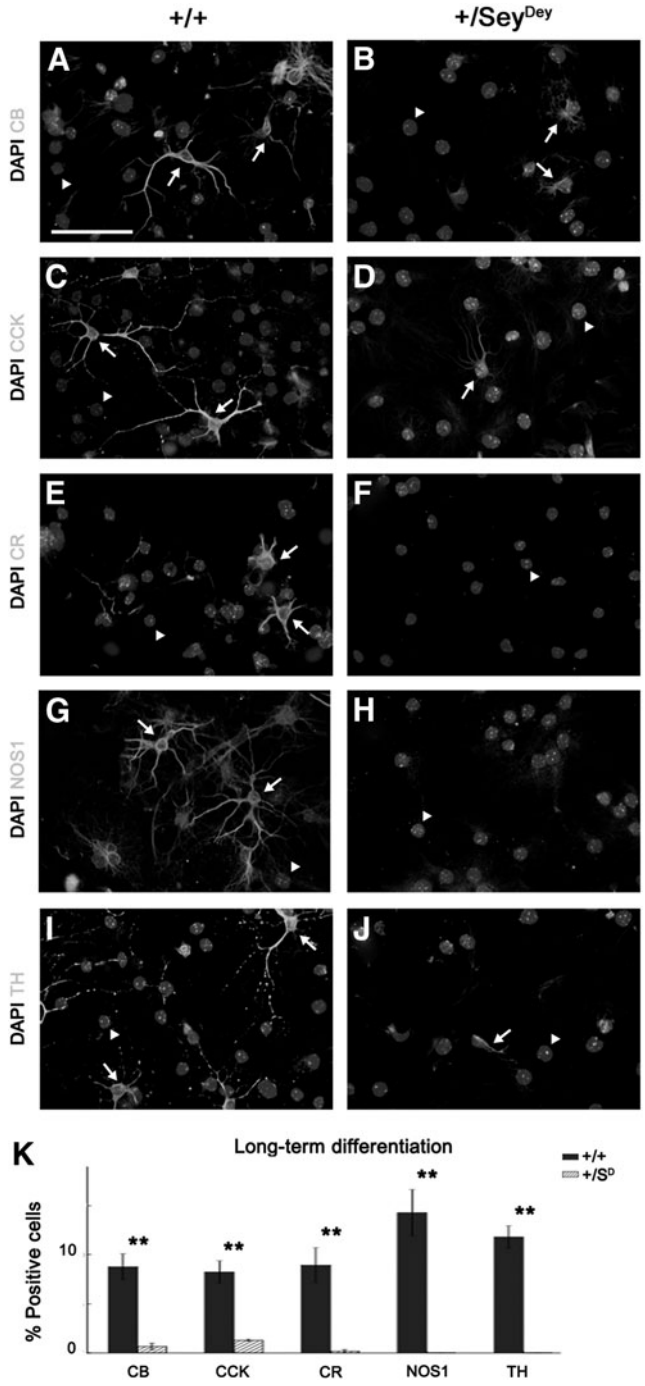

FIG. 7. The survival and differentiation of the main OB interneuron populations decreases in cultures from +/Sey^{Dey} aOBSCs. Wild-type aOBSCs cultured for 7 DIV in a medium composed of Dulbecco's modified Eagle's medium/F12/N2/B27 plus 2% fetal bovine serum and supplemented with a single dose of fibroblast growth factor-2 (FGF-2) generate CB$^+$, CCK$^+$, CR$^+$, NOS1$^+$, and TH$^+$ neurons (*arrows*: **A, C, E, G, I**). By contrast, NOS1- and TH$^+$ neurons were not detected in +/Sey^{Dey} aOBSC cultures growing under the same conditions, and the numbers of calbindin (CB), cholecystokinin (CCK) and calretinin (CR) were markedly reduced **(B, D, F, H, J)**, as shown in the graph **(K)**. *Arrowheads* point to DAPI nuclei. Results represent the mean ± SEM from at least three cultures per condition. Scale bar: 50 μm. $^{**}P$ value < 0.01.

the absence of significant changes in TUNEL$^+$ cells suggests that cells in +/Sey^{Dey} cultures probably died before they could be detected with the TUNEL assay at 7 DIV.

Since various neurochemical populations of OB interneurons were generated in the cultures, we evaluated by immunostaining the presence of CB$^+$, CCK$^+$, CR$^+$, NOS1$^+$, and TH$^+$ cells (Fig. 7, arrows). In wild-type cultures, CB$^+$ cells with different morphologies were generated, with most of them presenting one or two major dendrites along with dendritic branches (Fig. 7A). However, in +/Sey^{Dey} cultures, only stellate CB$^+$ cells with short dendrites were observed (Fig. 7B), and these cells were significantly less abundant than in +/+ cultures (Fig. 7K; $P < 0.001$). CCK$^+$ neurons were relatively big and complex cells in wild-type cultures, bearing 3 to 4 highly ramified dendrites (Fig. 7C). By contrast, +/Sey^{Dey} CCK$^+$ cells had fewer and shorter dendrites (Fig. 7D), and these cells were less common (Fig. 7K; $P < 0.001$). Unlike wild-type cultures, in which CR$^+$ neurons with a relatively immature morphology could be detected, CR$^+$ cells were virtually absent in the +/Sey^{Dey} cultures (Fig. 7E, F, K; $P < 0.001$). The immunostaining of NOS1$^+$ neurons reflected the complete depletion of this subpopulation in the +/Sey^{Dey} cultures, whereas they were relatively abundant (14% of all DAPI-positive cells) and morphologically complex in the wild-type cultures (Fig. 7G, H, K). Similarly, there were virtually no TH$^+$ cells in the Pax6 heterozygous cultures compared with their relative abundance in the wild-type cultures (11.8% of all DAPI-positive cells; Fig. 7I–K). These results indicate that Pax6 regulates the differentiation and/or survival of the major types of OB interneurons, and suggest that the TH$^+$, NOS1$^+$, and CR$^+$ populations are slightly more sensitive to Pax6 levels than CB and CCK neurons.

Pax6 haploinsufficiency causes a reduction in the arrival of newly generated cells in the OB and compromises the differentiation of distinct neurochemical neuronal subtypes

To investigate the physiological consequences of the +/Sey^{Dey} genotype on neuronal generation, differentiation, and survival in vivo, P75 +/+ and +/Sey^{Dey} mice were analyzed 15 days after having received an injection of BrdU to assess the arrival and differentiation of newly generated cells in the OB [48] or 60 days after the BrdU injection to analyze their long-term survival and neurochemical phenotype (Fig. 8). When total cell number was estimated by means of a stereological method, the large majority of cells labeled with BrdU in the GCL gave rise to neurons, as they were also labeled for NeuN at 15 dpi (+/+, 95.35% ± 2.39%; +/Sey^{Dey}, 88.43% ± 2.04%: $P = 0.093$) and at 60 dpi (+/+, 97.7% ± 1.18%: +/Sey^{Dey}, 96.98% ± 0.8%: $P = 0.616$).

After 15 dpi, the incorporation of newly generated BrdU$^+$ cells into the whole OB was significantly lower in the +/Sey^{Dey} mice than in the wt mice (Fig. 8A, B; $P < 0.001$). This 32% reduction in the incorporation of cells was equivalent to the volume loss observed in the OB of these mice (+/+, 4.66 ± 0.328 mm^3; +/Sey^{Dey}, 3.25 ± 0.095 mm^3: $P < 0.001$). The total number of new cells in the granule cell layer (GCL) and GL was also significantly reduced by 31% ($P < 0.01$) and 41.8% ($P < 0.001$), respectively, whereas no significant changes were observed in the EPL (Fig. 8A). Furthermore, the proportion of double-labeled BrdU and

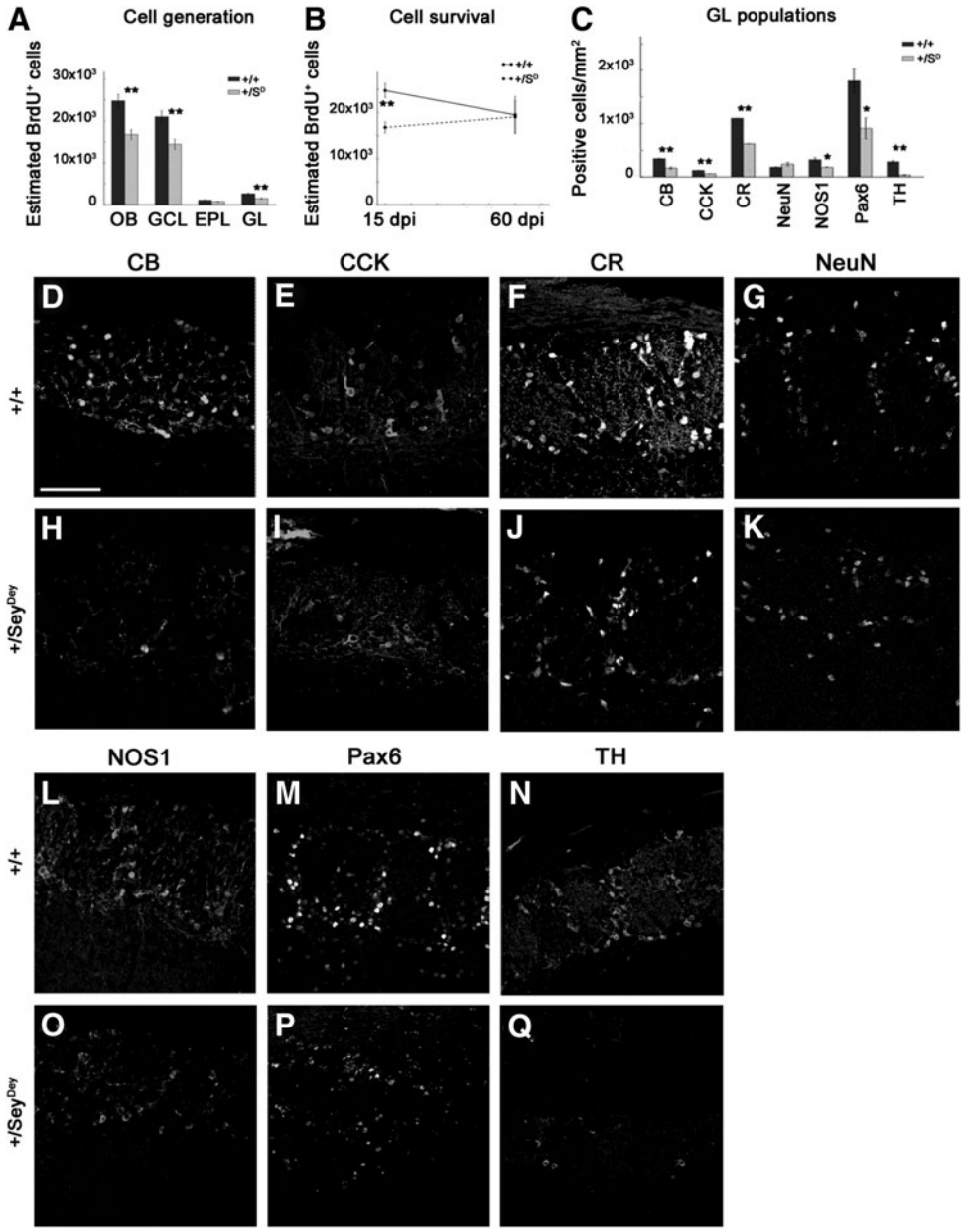

FIG. 8. The arrival of newly generated cells and the density of distinct periglomerular neurons is decreased in the OB of +/Sey^{Dey} mice. **(A)** The estimated total number of BrdU$^+$ cells at 15 days post-BrdU injection (dpi; P75–P90 mice) was reduced in the whole OB of +/Sey^{Dey} mice, as well as in the granule cell layer (GCL) and glomerular layer (GL). **(B)** Two months after the BrdU injections (P75–P135 mice; 60 dpi), the total number of newly generated cells in the OB of wild-type and +/Sey^{Dey} mice was similar. **(C)** In the +/Sey^{Dey} glomerular layer, lower densities (corrected by volume loss) of periglomerular neurons were found, as evident in the images. **(D–Q)** Immunostaining of OB coronal sections for CB **(D, H)**, CCK **(E, I)**, CR **(F, J)**, neuronal nuclear antigen (NeuN) **(G, K)**, NOS1 **(L, O)**, Pax6 **(M, P)** and tyrosine hydroxylase (TH) **(N, Q)** in +/+ **(D–G, L–N),** and +/Sey^{Dey} mice **(H–K, O–Q)**. The density of all populations was reduced in the +/Sey^{Dey} glomerular layer. Results represent the mean ± SEM from three to five animals per genotype. Scale bar: 50 μm. **P* value < 0.05; ***P* value < 0.01.

NeuN cells relative to the total NeuN population decreased by 33% in the GCL of the mutant mice at 15 dpi (+/+, 2.81% ± 0.24%; +/Sey^{Dey}, 1.89% ± 0.18%: $P < 0.05$). These findings suggest that neuronal generation and differentiation is negatively affected by the *Pax6* mutation.

To study the long-term survival of the cells, the mice were analyzed at 60 dpi and the data were compared with those obtained at 15 dpi. The estimated numbers of cells at 60 and 15 dpi were not statistically significant in either wt or +/Sey^{Dey} mice (Fig. 8B): wt 15 dpi: 24,590.1 ± 3,160.9; wt 60 dpi: 19,466.2 ± 9,855.4, $P = 0.279$; +/Sey^{Dey} 15 dpi: 17,528.9 ± 3,136.9; +/Sey^{Dey} 60 dpi: 19,031.3 ± 6,896.8, $P = 0.706$.

No significant differences between the +/Sey^{Dey} and wt in the number of BrdU$^+$ cells in the OB were found after 60 dpi (Fig. 8B), indicating that the effect of *Pax6* haploinsufficiency in the +/Sey^{Dey} mouse does not affect the long-term survival of the whole neuronal population. However, the percentage of new (BrdU$^+$) dopaminergic neurons in the GL, cells which were not detected at 15 dpi probably due to the longer time that these neurons require to differentiate, decreased 7.5-fold in the mutant mice at 60 dpi (+/+, 48.93% ± 11.86%; +/Sey^{Dey}, 6.46% ± 1.70%: $P < 0.05$). In contrast, the percentage of newly formed (BrdU$^+$) calbindin- and calretinin-positive neurons was similar in both mice genotypes at 60 dpi (calbindin: +/+, 33.09% ± 6.77%; +/Sey^{Dey}, 41.50% ± 8.36%: $P = 0.45$; calretinin: +/+, 39.6% ± 7.96%; +/Sey^{Dey}, 36.48% ± 4.01%: $P = 0.74$). These findings support a specific role of Pax6 in the differentiation and possibly survival of OB dopaminergic neuronal progenitors.

Reduced cell densities of different neurochemical interneuron populations in +/Sey^{Dey} mice in vivo

Having demonstrated the altered incorporation of newly generated cells in the *+/Sey^{Dey}* mouse OB in vivo, and the reduced survival and differentiation of the main OB

interneuron neurochemical subtypes in vitro, we examined the phenotype of the main OB interneuron subtypes by analyzing the expression of different neurochemical markers (CB, CCK, CR, NOS1, Pax6, and TH) by immunofluorescence in conjunction with the identification of neurons by their expression of NeuN (Figs. 8C–Q and 9). Accordingly, we analyzed the density of these interneuron subtypes in the GL and GCL of the OB, employing a corrected cell density value as the mutant OB had a smaller volume (see Materials and Methods section).

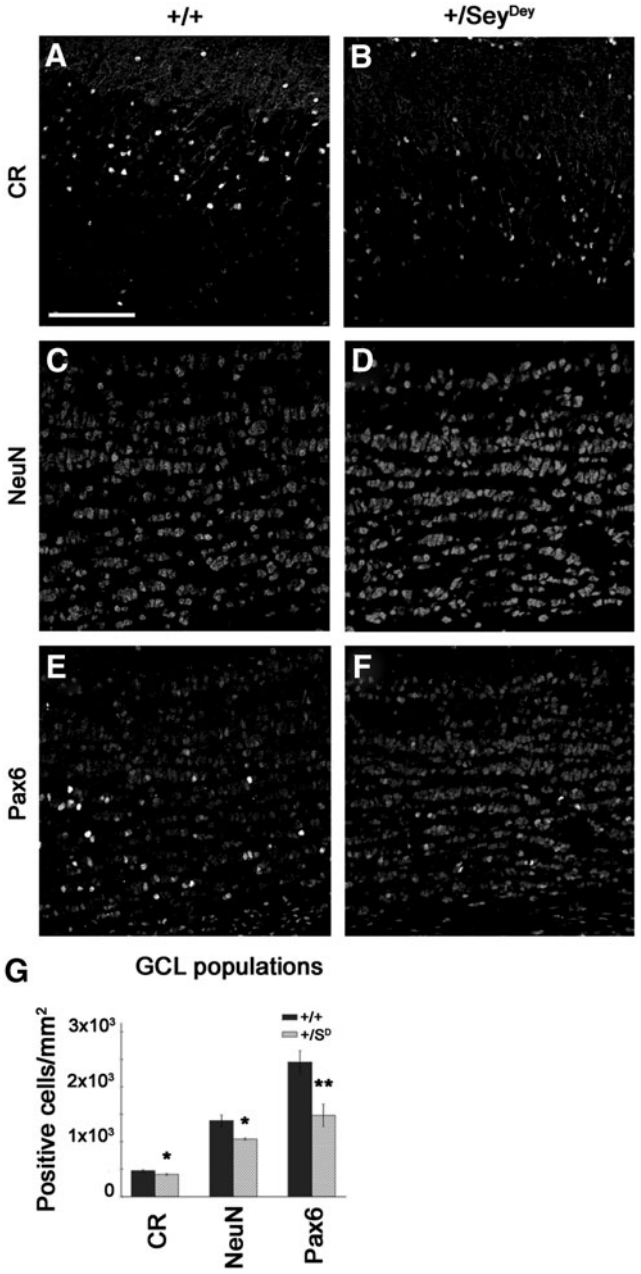

FIG. 9. The number of granule neurons is reduced in the $+/Sey^{Dey}$ olfactory bulb. Immunostaining for CR **(A, B)**, NeuN **(C, D),** and Pax6 **(E, F)** in coronal sections from the granule cell layer (GCL) of $+/+$ **(A, C, E)** and $+/Sey^{Dey}$ **(B, D, F)** OBs. Quantification of the cell density (corrected by volume loss) showed a decrease in the number of granule neuron populations in the mutant olfactory bulbs **(G)**. Results represent the mean ± SEM from three animals per genotype. Scale bar: 50 μm. *P value < 0.05; **P value < 0.01.

In the OB, the CB^+ interneuron population was composed exclusively of periglomerular neurons [31,66], and the density of this cell population was reduced by 51% in $+/Sey^{Dey}$ mice compared with wt mice (Fig. 8C, D, H; $P < 0.001$). The density of the CCK^+ cells was also reduced by 52% in *Pax6* heterozygous (Fig. 8C, E, I; $P < 0.001$). In fact, both the periglomerular and external tufted CCK populations [31,67] were reduced in the mutants (periglomerular: $+/+$, 34.06 ± 1.51 CCK^+/mm^2; $+/Sey^{Dey}$, 11.13 ± 1.32 CCK^+/mm^2: $P < 0.001$) (external tufted: $+/+$, 89.38 ± 3.81 CCK^+/mm^2; $+/Sey^{Dey}$: 47.27 ± 1.83 CCK^+/mm^2: $P < 0.001$).

CR is expressed in a subpopulation of PG and in granule neurons distributed in the superficial region of the granule cell layer [68]. The density of the CR periglomerular cells was lower in $+/Sey^{Dey}$ (43%) than in wild-type mice (Fig. 8C, F, J; $P < 0.001$), as was the density of CR granule cells in $+/Sey^{Dey}$ mutants, although to a lesser extent than in the GL (14%, $P < 0.05$; Fig. 9A, B, G). Nitrergic cells are found in all OB layers but they are especially abundant in the GL, where they are PGs, or superficial short axon (SSA) cells or external tufted neurons [69]. The density of $NOS1^+$ cells was also reduced in the $+/Sey^{Dey}$ compared with wild type (44%, $P < 0.05$; Fig. 8C, L, O).

Within the OB interneuron populations, Pax6 is expressed in dopaminergic (TH^+), CB^+, and CR^+ PGNs [6,31,33], and in a large subpopulation of granule cells. Indeed, in the $+/Sey^{Dey}$ mice, the density of Pax6-positive cells was reduced by 50% ($P < 0.01$) and 40% ($P < 0.01$) in the GL and GCL, respectively (Figs. 8C, M, P and 9E–G). Notably, the number of dopaminergic neurons was strongly affected by the $+/Sey^{Dey}$ mutation, which provoked a significant decrease in this neural phenotype (86%; $P < 0.001$). This was due to a severe reduction of TH^+ periglomerular neurons (94%, $P < 0.001$; Fig. 8C, N, Q), while the density of TH^+ SSA cells did not vary significantly ($+/+$, 13.77 ± 2.04 SSA TH^+/mm^2; $+/Sey^{Dey}$, 21.81 ± 3.45 SSA TH^+/mm^2: $P = 0.115$). Finally, *Pax6* haploinsufficiency also provoked a significant reduction in the total neuronal population labeled for NeuN in the GCL (Fig. 9C, D, G).

Taken together, our results indicate that the *Pax6* mutation in $+/Sey^{Dey}$ mice causes a reduction in the incorporation of newly generated neurons into the GCL and GL of the adult OB. Our in vivo and in vitro findings support a general role of Pax6 in controlling neuronal generation and differentiation from aOBSCs. Indeed, this TF appears to influence the differentiation and possibly survival of distinct neurochemical subtypes, with dopaminergic PG cells being extremely dependent on appropriate Pax6 levels.

Discussion

In this study, we set out to investigate the regulatory role of Pax6 in adult OB neurogenesis, focusing particularly on the control of aNSC number and differentiation both in vitro and in vivo. Our results indicate that *Pax6* haploinsufficiency in the $+/Sey^{Dey}$ mouse negatively affects the self-renewal and proliferation of aOBSCs in vitro, and that proliferation defects are also found in vivo, specifically in $Nestin^+$ cells, possibly reflecting a negative impact of the

mutation on NSC proliferation. However, a subpopulation of +/Sey^{Dey} progenitors has the capacity to expand, in part, similar to the wild-type ones. The differentiation potential of aOBSCs to generate oligodendrocytes and distinct classes of neurons in vitro was also impaired by the +/Sey^{Dey} mutation, while astrocyte differentiation was unaffected. In conjunction with the reduced neuronal generation and incorporation into the OB in vivo, these findings support a key role for Pax6 in the control of the generation of neuronal and glial cell diversity in the adult OB. While cell death was enhanced in proliferating *Pax6* haploinsufficient aOBSCs and during the differentiation process in cell culture, no obvious changes were observed in the long-term survival of newly generated neurons in vivo, except in that of dopaminergic neurons, suggesting that partial deficiency of Pax6 triggers cell death in a context-dependent manner.

It cannot be completely ruled out that deletions of the *Wt1* and *Rcn* genes in the +/Sey^{Dey} mutant mouse may also have an impact on the phenotypes observed, specifically in the formation of the OB. However, although the OB is reduced in size and it is hypocellular in homozygous KO mice for an alternative splice variant of *Wt1*, the heterozygous knockout mice for *Wt1* and *Rcn* appeared normal [44–47]. Accordingly, we suggest that the phenotypes observed in aOBSCs and in the OB of +/Sey^{Dey} mice in vivo can be primarily attributed to the heterozygous deletion of Pax6. In support of this, *Wt1* expression could not be detected in either control or mutant aOBSCs and the expression of *Rcn* did not apparently change in +/Sey^{Dey} cells, whereas the level of *Pax6* mRNA was reduced 2.6-fold in the mutant cells. Furthermore, we detected an upregulation of *Gsx2* in mutant aOBSCs, a gene known to be repressed by Pax6 [13,61].

Pax6 regulates the self-renewal, proliferation, survival, and differentiation of aOBSCs

Several authors have proposed a relationship between the regulation of the cell cycle and the dynamics of stem cell populations, including features such as self-renewal, cell fate choice, differentiation, and cell survival [70,71]. aOBSCs that are isolated from +/Sey^{Dey} heterozygous mice and grown in culture display defects in self-renewal, proliferation, multi-lineage differentiation, and survival. Our clonal analysis also shows that a number of single-plated cells which remained as single did not form neurospheres after 8 DIV, even in the presence of FGF-2 and EGF, indicating that Pax6 deficiency inhibits self-renewal of aOBSCs. However, our analyses also reveal that when +/Sey^{Dey} cells from primary spheres are disaggregated and plated they form secondary neurospheres although of a reduced size. We suggest that the mechanism underlying all these phenotypes could be related to the deregulation of the cell cycle machinery and of TF expression caused by the Pax6 deficiency in aOBSCs. Indeed, the levels of p21, p27, and p53 significantly decrease in proliferating +/Sey^{Dey} cells, whereas no detectable changes were found in the levels of key molecules of the PI3K/Akt and MAPK/Erk signaling pathways, both of which are critical for the survival and differentiation of NSCs [62]. Accordingly, Pax6 may activate self-renewal, maintenance, and multipotent differentiation of aOBSCs by directly modulating the cell cycle, an effect that could be deregulated in conditions of Pax6 deficiency. This interpretation would concur with the alterations to the cell cycle and to cell cycle molecular regulators in cortical and retinal progenitors of *Pax6* null embryonic mice. Indeed, during brain development, Pax6 influences the balance between self-renewal and differentiation of NSCs by controlling the cell cycle and the cell's ability to divide symmetrically or asymmetrically [21,23,24,27,55,56,58,72–75].

The molecular mechanisms underlying these actions are largely unknown but they might well be related to the G1/S phase transition. In fact, it has been reported that Pax6 can physically interact with phosphoRetinoblastoma (pRb) [76], and that different cyclin-dependent kinase inhibitors, as well as other cell cycle regulators, are also Pax6 transcriptional targets [23,24,72]. Whether changes in the Pax6-pRB interaction in aOBSCs, and possibly in other interactions, might be involved in the alteration of self-renewal and survival, and in the diminished differentiation of these cells, requires further study. Surprisingly, the levels of cell cycle inhibitors p21, p27, and p53 [63–65,77] were reduced in proliferative +/Sey^{Dey} cells at 4 DIV, which was concomitant with a reduction rather than an increase in aOBSC proliferation. However, we hypothesize that the reduced levels of cell cycle inhibitors could be a mechanism to compensate for the loss of Pax6 and its negative effects on the cell cycle. This may explain why a subpopulation of aOBSCs and progenitors deficient in Pax6 are able to proliferate and form clonal secondary neurospheres. Reduced levels of cell cycle inhibitors could also increase cell death and reduce neuronal differentiation, as previously reported in the SVZ of p27 KO mice [65], as well as promote astrocyte differentiation, as reported for NSCs lacking p21 [77].

In addition to the changes in cell cycle regulators, the upregulation of *Gsx2* in +/Sey^{Dey} cells maybe involved in the partially altered aOBSC self-renewal. Indeed, we previously showed that high levels of *Gsx2* inhibit OBSC self-renewal. Furthermore, in the light of studies from other laboratories, we suggest that the upregulation of *Gsx2* in the mutant cells can be attributed to the reduced levels of *Pax6* [12,13,61].

As mentioned earlier, the differentiation and survival of the newly generated cells from +/Sey^{Dey} aOBSCs is severely altered. Notably, our time course analysis of aOBSC differentiation suggests that distinct mechanisms may operate depending on whether the cell is differentiating into the neuronal, astrocyte, or oligodendrocyte lineages. Indeed, although at 1 and 2 DIV there is a marked reduction in the proportion of TuJ1$^+$ immature neurons in +/Sey^{Dey} cultures compared with controls, the proportion of neuronal cells increases from 1 to 2 DIV in both control and +/Sey^{Dey} cultures. Hence, the Pax6 mutation does not appear to completely block the generation and survival of aOBSC-derived neurons. By contrast, the proportions of O4$^+$ oligodendrocytes in the +/Sey^{Dey} cultures were extremely and similarly low at 1 and 2 DIV, indicating that Pax6 haploinsufficiency almost fully impedes the generation and survival of oligodendrocytes from aOBSCs. Conversely, the proportion of astrocytes was not significantly affected in the +/Sey^{Dey} cultures, supporting the view that a full dosage of Pax6 is not required for the initial differentiation and survival of astrocytes from aOBSCs. Our findings support the notion that Pax6 levels control not only neurogenesis [23,24,28–30,40,75,78] but also the multipotent cell fate of aOBSCs. Although this role of Pax6 could extend to other

NSC populations, it appears to be modulated in a cell- and/or genetic context. In fact, NSCs isolated from the embryonic forebrain of *Pax6* conditional KO mice showed both reduced oligodendrocyte and astrocyte differentiation [20], whereas NSC/progenitors isolated from the embryonic forebrain of *Pax6* heterozygous (+/Sey) and homozygous (Sey/Sey) rats and mice developed excessive numbers of immature astrocytes [22,42].

Pax6 regulates the incorporation of new neurons into the adult OB

We show here that *Pax6* haploinsufficiency in the +/Sey^{Dey} mutant causes a reduction in the arrival of newly generated cells to the OB. Given that the large majority of the BrdU$^+$ cells express NeuN (88%–95%), and that the proportion of double-labeled BrdU/NeuN cells in the total NeuN population was significantly lower in the mutants, our results suggest a key role for Pax6 in the incorporation of new neurons in the OB. Hence, neuron generation and replacement in the adult OB would appear to be negatively affected by the *Pax6* heterozygosis. The role of Pax6 in neuronal generation and differentiation was also found in vitro in which dopaminergic neurons were nearly absent in cultures from +/Sey^{Dey} aOBSCs and other neuronal populations were also severely affected; effects that could also be dependent on the increased cell death detected in +/Sey^{Dey} cultures.

Our results are consistent with previous findings and emphasize that a full dosage of this TF is necessary for neuronal generation and survival in the adult OB [6,32,35,37,38,79]. Moreover, we show that the rostral SVZ of +/Sey^{Dey} mice contains more cells (with fewer proliferative cells) than that of controls, suggesting that cell exit from the SVZ is partially impaired and that, therefore, cells tend to accumulate in this zone, decreasing neuronal incorporation into the OB. Since defects in neuronal migration were not found in the SVZ-RMS of mice bearing a point mutation in the Pax6 homeodomain that abolishes DNA binding [38], we hypothesize that the paired domain of Pax6 may be involved in the regulation of neuroblast exit from the SVZ. Conversely, no changes were observed in the distribution of newly generated cells in the OB of +/Sey^{Dey} mutant mice, suggesting that neuronal migration within the OB was not altered by Pax6 deficiency. In the +/Sey^{Dey} mice, the number of newly generated dopaminergic neurons was significantly decreased at 60 dpi, suggesting that these neurons and/or their neuronal progenitors are highly dependent on Pax6 levels. In contrast, the long-term survival of newly generated CB$^+$ and CR$^+$ neurons was apparently similar to that of control mice. However, the densities of these and other neuronal populations were reduced in the OB, probably as a result of altered neuronal generation and survival during the embryonic period, supporting the role of Pax6 as key neurogenic TF during development.

In conclusion, our results indicate that the *Pax6* haploinsufficiency in +/Sey^{Dey} mice produces a reduction in the incorporation of newly generated neurons into the adult OB. They also suggest a role for this TF in the differentiation and survival of distinct neurochemical interneuron subtypes from aOBSCs, Furthermore, our findings support a general role of Pax6 in the regulation of aOBSC maintenance, and multi-lineage differentiation through the control of the cell cycle molecular machinery and the expression of key TFs.

Acknowledgments

This work was funded by grants from the Spanish Ministerio de Ciencia e Innovación and Ministerio de Economía y Competitividad (MICINN and MINECO; BFU2007-61230 and BFU2010-1963), the Instituto de Salud Carlos III (ISCIII; CIBERNED CB06/05/0065), and the Comunidad de Madrid (S2012/BMD-2336) to C.V.-A., and by grants from Ministerio de Ciencia y Tecnología (BFU2010-18284), Ministerio de Sanidad, Política Social e Igualdad (Plan Nacional Sobre Drogas), Junta de Castilla y León, Centro en Red de Medicina Regenerativa y Terapia Celular de Castilla y León y Fundación Memoria D. Samuel Solórzano-Barruso to J.R.A. and E.W. G.G.C., V.N.-E., and A.H.-C. were supported by a FPI. Fellowship from the MICINN and MINECO. G.G.C. was the recipient of a short-term fellowship from the Red Olfativa Española.

Author Disclosure Statement

The authors have no competing financial interests to declare.

References

1. Merkle FT, Z Mirzadeh and A Alvarez-Buylla. (2007). Mosaic organization of neural stem cells in the adult brain. Science 317:381–384.
2. Brill MS, J Ninkovic, E Winpenny, RD Hodge, I Ozen, R Yang, A Lepier, S Gascon, F Erdelyi, et al. (2009). Adult generation of glutamatergic olfactory bulb interneurons. Nat Neurosci 12:1524–1533.
3. Lois C and A Alvarez-Buylla. (1994). Long-distance neuronal migration in the adult mammalian brain. Science 264:1145–1148.
4. Giachino C and V Taylor. (2009). Lineage analysis of quiescent regenerative stem cells in the adult brain by genetic labelling reveals spatially restricted neurogenic niches in the olfactory bulb. Eur J Neurosci 30:9–24.
5. Gritti A, L Bonfanti, F Doetsch, I Caille, A Alvarez-Buylla, DA Lim, R Galli, JM Verdugo, DG Herrera and AL Vescovi. (2002). Multipotent neural stem cells reside into the rostral extension and olfactory bulb of adult rodents. J Neurosci 22:437–445.
6. Hack MA, A Saghatelyan, A de Chevigny, A Pfeifer, R Ashery-Padan, PM Lledo and M Gotz. (2005). Neuronal fate determinants of adult olfactory bulb neurogenesis. Nat Neurosci 8:865–872.
7. Liu Z and LJ Martin. (2003). Olfactory bulb core is a rich source of neural progenitor and stem cells in adult rodent and human. J Comp Neurol 459:368–391.
8. Moreno-Estellés M, P Gonzalez-Gomez, R Hortiguela, M Diaz-Moreno, J San Emeterio, AL Carvalho, I Fariñas and H Mira. (2012). Symmetric expansion of neural stem cells from the adult olfactory bulb is driven by astrocytes via WNT7A. Stem Cells 30:2796–2809.
9. Vergaño-Vera E, HR Méndez-Gómez, A Hurtado-Chong, JC Cigudosa and C Vicario-Abejón. (2009). Fibroblast growth factor-2 increases the expression of neurogenic genes and promotes the migration and differentiation of neurons derived from transplanted neural stem/progenitor cells. Neuroscience 162:39–54.
10. Nieto-Estévez V, J Pignatelli, MJ Arauzo-Bravo, A Hurtado-Chong and C Vicario-Abejón. (2013). A global transcriptome analysis reveals molecular hallmarks of neural

stem cell death, survival, and differentiation in response to partial FGF-2 and EGF deprivation. PLoS One 8: e53594.
11. Marei HE, AE Ahmed, F Michetti, M Pescatori, R Pallini, P Casalbore, C Cenciarelli and M Elhadidy. (2012). Gene expression profile of adult human olfactory bulb and embryonic neural stem cell suggests distinct signaling pathways and epigenetic control. PLoS One 7:e33542.
12. Díaz-Guerra E, J Pignatelli, V Nieto-Estévez and C Vicario-Abejón. (2013). Transcriptional regulation of olfactory bulb neurogenesis. Anat Rec (Hoboken) 296:1364–1382.
13. Carney RS, LA Cocas, T Hirata, K Mansfield and JG Corbin. (2009). Differential regulation of telencephalic pallial-subpallial boundary patterning by Pax6 and Gsh2. Cereb Cortex 19:745–759.
14. Stoykova A and P Gruss. (1994). Roles of Pax-genes in developing and adult brain as suggested by expression patterns. J Neurosci 14(Pt 2):1395–1412.
15. Georgala PA, M Manuel and DJ Price. (2011). The generation of superficial cortical layers is regulated by levels of the transcription factor Pax6. Cereb Cortex 21:81–94.
16. Hirata T, T Nomura, Y Takagi, Y Sato, N Tomioka, H Fujisawa and N Osumi. (2002). Mosaic development of the olfactory cortex with Pax6-dependent and -independent components. Brain Res Dev Brain Res 136:17–26.
17. Jimenez D, C Garcia, F de Castro, A Chedotal, C Sotelo, JA de Carlos, F Valverde and L Lopez-Mascaraque. (2000). Evidence for intrinsic development of olfactory structures in Pax-6 mutant mice. J Comp Neurol 428:511–526.
18. Sisodiya SM, SL Free, KA Williamson, TN Mitchell, C Willis, JM Stevens, BE Kendall, SD Shorvon, IM Hanson, AT Moore and V van Heyningen. (2001). PAX6 haploinsufficiency causes cerebral malformation and olfactory dysfunction in humans. Nat Genet 28:214–216.
19. Berger J, S Berger, TC Tuoc, M D'Amelio, F Cecconi, JA Gorski, KR Jones, P Gruss and A Stoykova. (2007). Conditional activation of Pax6 in the developing cortex of transgenic mice causes progenitor apoptosis. Development 134:1311–1322.
20. Gomez-Lopez S, O Wiskow, R Favaro, SK Nicolis, DJ Price, SM Pollard and A Smith. (2011). Sox2 and Pax6 maintain the proliferative and developmental potential of gliogenic neural stem cells in vitro. Glia 59:1588–1599.
21. Hsieh YW and XJ Yang. (2009). Dynamic Pax6 expression during the neurogenic cell cycle influences proliferation and cell fate choices of retinal progenitors. Neural Dev 4:32.
22. Sakayori N, T Kikkawa and N Osumi. (2012). Reduced proliferation and excess astrogenesis of Pax6 heterozygous neural stem/progenitor cells. Neurosci Res 74: 116–121.
23. Sansom SN, DS Griffiths, A Faedo, DJ Kleinjan, Y Ruan, J Smith, V van Heyningen, JL Rubenstein and FJ Livesey. (2009). The level of the transcription factor Pax6 is essential for controlling the balance between neural stem cell self-renewal and neurogenesis. PLoS Genet 5:e1000511.
24. Osumi N, H Shinohara, K Numayama-Tsuruta and M Maekawa. (2008). Concise review: Pax6 transcription factor contributes to both embryonic and adult neurogenesis as a multifunctional regulator. Stem Cells 26:1663–1672.
25. Marquardt T, R Ashery-Padan, N Andrejewski, R Scardigli, F Guillemot and P Gruss. (2001). Pax6 is required for the multipotent state of retinal progenitor cells. Cell 105: 43–55.
26. Wen J, Q Hu, M Li, S Wang, L Zhang, Y Chen and L Li. (2008). Pax6 directly modulate Sox2 expression in the neural progenitor cells. Neuroreport 19:413–417.
27. Quinn JC, M Molinek, BS Martynoga, PA Zaki, A Faedo, A Bulfone, RF Hevner, JD West and DJ Price. (2007). Pax6 controls cerebral cortical cell number by regulating exit from the cell cycle and specifies cortical cell identity by a cell autonomous mechanism. Dev Biol 302:50–65.
28. Maekawa M, N Takashima, Y Arai, T Nomura, K Inokuchi, S Yuasa and N Osumi. (2005). Pax6 is required for production and maintenance of progenitor cells in postnatal hippocampal neurogenesis. Genes Cells 10:1001–1014.
29. Klempin F, RA Marr and DA Peterson. (2012). Modification of pax6 and olig2 expression in adult hippocampal neurogenesis selectively induces stem cell fate and alters both neuronal and glial populations. Stem Cells 30:500–509.
30. Ninkovic J, A Steiner-Mezzadri, M Jawerka, U Akinci, G Masserdotti, S Petricca, J Fischer, A von Holst, J Beckers, et al. (2013). The BAF complex interacts with Pax6 in adult neural progenitors to establish a neurogenic cross-regulatory transcriptional network. Cell Stem Cell 13:403–418.
31. Baltanas FC, E Weruaga, AR Murias, C Gomez, GG Curto and JR Alonso. (2009). Chemical characterization of Pax6-immunoreactive periglomerular neurons in the mouse olfactory bulb. Cell Mol Neurobiol 29:1081–1085.
32. Haba H, T Nomura, F Suto and N Osumi. (2009). Subtype-specific reduction of olfactory bulb interneurons in Pax6 heterozygous mutant mice. Neurosci Res 65:116–121.
33. Hurtado-Chong A, MJ Yusta-Boyo, E Vergaño-Vera, A Bulfone, F de Pablo and C Vicario-Abejón. (2009). IGF-I promotes neuronal migration and positioning in the olfactory bulb and the exit of neuroblasts from the subventricular zone. Eur J Neurosci 30:742–755.
34. de Chevigny A, N Core, P Follert, S Wild, A Bosio, K Yoshikawa, H Cremer and C Beclin. (2012). Dynamic expression of the pro-dopaminergic transcription factors Pax6 and Dlx2 during postnatal olfactory bulb neurogenesis. Front Cell Neurosci 6:6.
35. Kohwi M, N Osumi, JL Rubenstein and A Alvarez-Buylla. (2005). Pax6 is required for making specific subpopulations of granule and periglomerular neurons in the olfactory bulb. J Neurosci 25:6997–7003.
36. Brill MS, M Snapyan, H Wohlfrom, J Ninkovic, M Jawerka, GS Mastick, R Ashery-Padan, A Saghatelyan, B Berninger and M Gotz. (2008). A dlx2- and pax6-dependent transcriptional code for periglomerular neuron specification in the adult olfactory bulb. J Neurosci 28:6439–6452.
37. de Chevigny A, N Core, P Follert, M Gaudin, P Barbry, C Beclin and H Cremer. (2012). miR-7a regulation of Pax6 controls spatial origin of forebrain dopaminergic neurons. Nat Neurosci 15:1120–1126.
38. Ninkovic J, L Pinto, S Petricca, A Lepier, J Sun, MA Rieger, T Schroeder, A Cvekl, J Favor and M Gotz. (2010). The transcription factor Pax6 regulates survival of dopaminergic olfactory bulb neurons via crystallin alphaA. Neuron 68:682–694.
39. Hack MA, M Sugimori, C Lundberg, M Nakafuku and M Gotz. (2004). Regionalization and fate specification in neurospheres: the role of Olig2 and Pax6. Mol Cell Neurosci 25:664–678.
40. Heins N, P Malatesta, F Cecconi, M Nakafuku, KL Tucker, MA Hack, P Chapouton, YA Barde and M Gotz. (2002).

Glial cells generate neurons: the role of the transcription factor Pax6. Nat Neurosci 5:308–315.
41. Kallur T, R Gisler, O Lindvall and Z Kokaia. (2008). Pax6 promotes neurogenesis in human neural stem cells. Mol Cell Neurosci 38:616–628.
42. Sakurai K and N Osumi. (2008). The neurogenesis-controlling factor, Pax6, inhibits proliferation and promotes maturation in murine astrocytes. J Neurosci 28: 4604–4612.
43. Ellison-Wright Z, I Heyman, I Frampton, K Rubia, X Chitnis, I Ellison-Wright, SC Williams, J Suckling, A Simmons and E Bullmore. (2004). Heterozygous PAX6 mutation, adult brain structure and fronto-striato-thalamic function in a human family. Eur J Neurosci 19:1505–1512.
44. Kent J, M Lee, A Schedl, S Boyle, J Fantes, M Powell, N Rushmere, C Abbott, V van Heyningen and WA Bickmore. (1997). The reticulocalbin gene maps to the WAGR region in human and to the small eye Harwell deletion in mouse. Genomics 42:260–267.
45. Theiler K, DS Varnum and LC Stevens. (1978). Development of Dickie's small eye, a mutation in the house mouse. Anat Embryol (Berl) 155:81–86.
46. Theiler K, DS Varnum and LC Stevens. (1980). Development of Dickie's small eye: an early lethal mutation in the house mouse. Anat Embryol (Berl) 161:115–120.
47. Wagner N, KD Wagner, A Hammes, KM Kirschner, VP Vidal, A Schedl and H Scholz. (2005). A splice variant of the Wilms' tumour suppressor Wt1 is required for normal development of the olfactory system. Development 132: 1327–1336.
48. Valero J, E Weruaga, AR Murias, JS Recio, GG Curto, C Gomez and JR Alonso. (2007). Changes in cell migration and survival in the olfactory bulb of the pcd/pcd mouse. Dev Neurobiol 67:839–859.
49. Baltanás FC, GG Curto, C Gomez, D Diaz, AR Murias, C Crespo, F Erdelyi, G Szabo, JR Alonso and E Weruaga. (2011). Types of cholecystokinin-containing periglomerular cells in the mouse olfactory bulb. J Neurosci Res 89:35–43.
50. Gómez C, GG Curto, FC Baltanas, J Valero, E O'Shea, MI Colado, D Diaz, E Weruaga and JR Alonso. (2012). Changes in the serotonergic system and in brain-derived neurotrophic factor distribution in the main olfactory bulb of pcd mice before and after mitral cell loss. Neuroscience 201:20–33.
51. Weruaga E, JG Brinon, A Porteros, R Arevalo, J Aijon and JR Alonso. (2000). Expression of neuronal nitric oxide synthase/NADPH-diaphorase during olfactory deafferentation and regeneration. Eur J Neurosci 12:1177–1193.
52. Román-Trufero M, HR Mendez-Gomez, C Perez, A Hijikata, Y Fujimura, T Endo, H Koseki, C Vicario-Abejón and M Vidal. (2009). Maintenance of undifferentiated state and self-renewal of embryonic neural stem cells by Polycomb protein Ring1B. Stem Cells 27:1559–1570.
53. Schmittgen TD and KJ Livak. (2008). Analyzing real-time PCR data by the comparative C(T) method. Nat Protoc 3:1101–1108.
54. Petreanu L and A Alvarez-Buylla. (2002). Maturation and death of adult-born olfactory bulb granule neurons: role of olfaction. J Neurosci 22:6106–6113.
55. Estivill-Torrus G, H Pearson, V van Heyningen, DJ Price and P Rashbass. (2002). Pax6 is required to regulate the cell cycle and the rate of progression from symmetrical to asymmetrical division in mammalian cortical progenitors. Development 129:455–466.
56. Manuel M, PA Georgala, CB Carr, S Chanas, DA Kleinjan, B Martynoga, JO Mason, M Molinek, J Pinson, et al. (2007). Controlled overexpression of Pax6 in vivo negatively autoregulates the Pax6 locus, causing cell-autonomous defects of late cortical progenitor proliferation with little effect on cortical arealization. Development 134:545–555.
57. Tamai H, H Shinohara, T Miyata, K Saito, Y Nishizawa, T Nomura and N Osumi. (2007). Pax6 transcription factor is required for the interkinetic nuclear movement of neuroepithelial cells. Genes Cells 12:983–996.
58. Warren N, D Caric, T Pratt, JA Clausen, P Asavaritikrai, JO Mason, RE Hill and DJ Price. (1999). The transcription factor, Pax6, is required for cell proliferation and differentiation in the developing cerebral cortex. Cereb Cortex 9:627–635.
59. Fuentealba LC, K Obernier and A Alvarez-Buylla. (2012). Adult neural stem cells bridge their niche. Cell Stem Cell 10:698–708.
60. Marqués-Torrejón MA, E Porlan, A Banito, E Gomez-Ibarlucea, AJ Lopez-Contreras, O Fernandez-Capetillo, A Vidal, J Gil, J Torres and I Fariñas. (2013). Cyclin-dependent kinase inhibitor p21 controls adult neural stem cell expansion by regulating Sox2 gene expression. Cell Stem Cell 12:88–100.
61. Méndez-Gómez HR and C Vicario-Abejón. (2012). The homeobox gene Gsx2 regulates the self-renewal and differentiation of neural stem cells and the cell fate of postnatal progenitors. PLoS One 7:e29799.
62. Otaegi G, MJ Yusta-Boyo, E Vergaño-Vera, HR Méndez-Gómez, AC Carrera, JL Abad, M González, EJ de la Rosa, C Vicario-Abejón and F de Pablo. (2006). Modulation of the PI 3-kinase-Akt signalling pathway by IGF-I and PTEN regulates the differentiation of neural stem/precursor cells. J Cell Sci 119(Pt 13):2739–2748.
63. Armesilla-Diaz A, P Bragado, I Del Valle, E Cuevas, I Lazaro, C Martin, JC Cigudosa and A Silva. (2009). p53 regulates the self-renewal and differentiation of neural precursors. Neuroscience 158:1378–1389.
64. Kippin TE, DJ Martens and D van der Kooy. (2005). p21 loss compromises the relative quiescence of forebrain stem cell proliferation leading to exhaustion of their proliferation capacity. Genes Dev 19:756–767.
65. Doetsch F, JM Verdugo, I Caille, A Alvarez-Buylla, MV Chao and P Casaccia-Bonnefil. (2002). Lack of the cell-cycle inhibitor p27Kip1 results in selective increase of transit-amplifying cells for adult neurogenesis. J Neurosci 22:2255–2264.
66. Kosaka T and K Kosaka. (2010). Heterogeneity of calbindin-containing neurons in the mouse main olfactory bulb: I. General description. Neurosci Res 67:275–292.
67. Gutierrez-Mecinas M, C Crespo, JM Blasco-Ibanez, FJ Gracia-Llanes, AI Marques-Mari and FJ Martinez-Guijarro. (2005). Characterization of somatostatin- and cholecystokinin-immunoreactive periglomerular cells in the rat olfactory bulb. J Comp Neurol 489:467–479.
68. Kosaka K, Y Aika, K Toida, CW Heizmann, W Hunziker, DM Jacobowitz, I Nagatsu, P Streit, TJ Visser and T Kosaka. (1995). Chemically defined neuron groups and their subpopulations in the glomerular layer of the rat main olfactory bulb. Neurosci Res 23:73–88.
69. Crespo C, FJ Gracia-Llanes, JM Blasco-Ibanez, M Gutierrez-Mecinas, AI Marques-Mari and FJ Martinez-Guijarro. (2003). Nitric oxide synthase containing periglomerular cells

are GABAergic in the rat olfactory bulb. Neurosci Lett 349:151–154.
70. Dehay C and H Kennedy. (2007). Cell-cycle control and cortical development. Nat Rev Neurosci 8:438–450.
71. Salomoni P and F Calegari. (2010). Cell cycle control of mammalian neural stem cells: putting a speed limit on G1. Trends Cell Biol 20:233–243.
72. Duparc RH, M Abdouh, J David, M Lepine, N Tetreault and G Bernier. (2007). Pax6 controls the proliferation rate of neuroepithelial progenitors from the mouse optic vesicle. Dev Biol 301:374–387.
73. Mi D, CB Carr, PA Georgala, YT Huang, MN Manuel, E Jeanes, E Niisato, SN Sansom, FJ Livesey, et al. (2013). Pax6 exerts regional control of cortical progenitor proliferation via direct repression of Cdk6 and hypophosphorylation of pRb. Neuron 78:269–284.
74. Nikoletopoulou V, N Plachta, ND Allen, L Pinto, M Gotz and YA Barde. (2007). Neurotrophin receptor-mediated death of misspecified neurons generated from embryonic stem cells lacking Pax6. Cell Stem Cell 1:529–540.
75. Walcher T, Q Xie, J Sun, M Irmler, J Beckers, T Ozturk, D Niessing, A Stoykova, A Cvekl, J Ninkovic and M Gotz. (2013). Functional dissection of the paired domain of Pax6 reveals molecular mechanisms of coordinating neurogenesis and proliferation. Development 140:1123–1136.
76. Cvekl A, Y Yang, BK Chauhan and K Cveklova. (2004). Regulation of gene expression by Pax6 in ocular cells: a case of tissue-preferred expression of crystallins in lens. Int J Dev Biol 48:829–844.
77. Porlan E, JM Morante-Redolat, MA Marques-Torrejon, C Andreu-Agullo, C Carneiro, E Gomez-Ibarlucea, A Soto, A Vidal, SR Ferron and I Fariñas. (2013). Transcriptional repression of Bmp2 by p21(Waf1/Cip1) links quiescence to neural stem cell maintenance. Nat Neurosci 16:1567–1575.
78. Jang ES and JE Goldman. (2011). Pax6 expression is sufficient to induce a neurogenic fate in glial progenitors of the neonatal subventricular zone. PLoS One 6: e20894.
79. Diaz D, C Gomez, R Munoz-Castaneda, F Baltanas, JR Alonso and E Weruaga. (2013). The olfactory system as a puzzle: playing with its pieces. Anat Rec (Hoboken) 296: 1383–1400.

Address correspondence to:
Dr. Carlos Vicario-Abejón
Instituto Cajal
Consejo Superior de Investigaciones Científicas (CSIC)
Avenida Doctor Arce 37
Madrid E-28002
Spain

E-mail: cvicario@cajal.csic.es

Received for publication January 28, 2014
Accepted after revision August 12, 2014
Prepublished on Liebert Instant Online August 12, 2014